Reduced-Order Framework for Exponential Stabilization of Periodic Orbits on Parameterized Hybrid Zero Dynamics Manifolds: Application to Bipedal Locomotion

Kaveh Akbari Hamed[a,*], Jessy W. Grizzle[b]

[a] *Department of Mechanical Engineering, San Diego State University, San Diego, CA 92182-1323 USA*

[b] *Department of Electrical Engineering and Computer Science, University of Michigan, Ann Arbor, MI 48109-2122, USA*

Abstract

This paper shows how controlled-invariant manifolds in hybrid dynamical systems can be used to reduce the offline computational burden associated with locally exponentially stabilizing periodic orbits. We recently introduced a method to systematically select stabilizing feedback controllers for hybrid periodic orbits from a family of parameterized control laws by solving offline optimization problems. These problems search for controller parameters as well as a set of Lyapunov matrices for the full-order hybrid systems. When the method is applied to mechanical systems with high degrees of freedom (DOF), the number of entries in the Lyapunov matrices may render the numerical optimization problems prohibitively slow. To address this challenge, the paper considers a family of attractive and parameterized hybrid zero dynamics (HZD) manifolds in the state space. It then investigates the properties of the associated Poincaré map to translate the full-order optimization framework to a reduced-order one on the parameterized HZD manifolds with lower-dimensional Lyapunov matrices. In addition, the paper provides a systematic approach to numerically compute the Jacobian linearization

*Corresponding Author

Email addresses: kakbarihamed@mail.sdsu.edu (Kaveh Akbari Hamed), grizzle@umich.edu (Jessy W. Grizzle)

URL: http://www-rohan.sdsu.edu/~kavehah/ (Kaveh Akbari Hamed), http://web.eecs.umich.edu/~grizzle/ (Jessy W. Grizzle)

of the parameterized Poincaré map on the HZD manifolds. The power of the proposed framework is demonstrated by designing a set of stabilizing input-output linearizing controllers for walking gaits of an underactuated 3D bipedal robot with 13 DOFs and 6 actuators. It is shown that the number of decision variables in the reduced-order optimization problem can be reduced by 70% compared to the full-order one.

Keywords: Hybrid Periodic Orbits, Hybrid Zero Dynamics Manifolds, Reduced-Order Exponential Stabilization Problem, Poincaré Map, Underactuated Bipedal Robots

---

1. Introduction

This paper presents a systematic framework to reduce the computational burden in the design of feedback controllers that render periodic orbits of hybrid dynamical systems locally exponentially stable. By investigating properties of the Poincaré map, the paper breaks down the exponential stabilization problem of hybrid periodic orbits for full-order models into a lower-dimensional one defined for a family of parameterized zero dynamics models. The framework can ameliorate specific challenges in the design of stabilizing controllers for bipedal robots arising from high dimensionality and underactuation. Specifically, the theoretical innovations are applied to design nonlinear stabilizing controllers for walking gaits of an underactuated 3D bipedal robot with 13 degrees of freedom (DOFs) and 6 actuators. It is shown that the number of decision variables for the lower-dimensional problem is reduced by 70% compared to the one for the full-order model.

Models of bipedal walking robots are hybrid with continuous-time phases to represent the right and left stance phases and discrete-time phases to represent the contact of the swing leg end with the walking surface [1, 2, 3, 4, 5, 6, 7, 8, 9, 10, 11, 12, 13, 14, 15, 16, 17]. Our motivation is to design stabilizing feedback controllers for 3D bipedal robots with high degrees of freedom and underactuation, but the results we present apply to a broader range of hybrid dynamical systems [18, 19, 20, 21].

The most basic tool for analyzing the stability of hybrid periodic orbits is the Poincaré return map that describes the evolution of the hybrid model on a hypersurface transversal to the orbits, referred to as the Poincaré section [2, 18, 22, 23]. An important drawback, however, is that in almost all practical

cases, there is *no* closed-form expression for the Poincaré map and it must be estimated *numerically*.

Previous work on bipedal walking has made use of a multi-level feedback control architecture in which parameters of a continuous-time controller were updated in an event-based manner to achieve stable bipedal walking [24, 25, 10, 26, 27, 28, 29, 30, 31, 32, 17, 33, 34]. One drawback of achieving stability via event-based controllers is the potentially large delay between the occurrence of a disturbance and the event-based control effort in the next steps. We have recently presented a systematic method to design continuous-time controllers that provide robust stability of a given periodic orbit without relying on event-based controllers [35, 36, 37]. This approach was numerically and experimentally illustrated to design nonlinear stabilizing controllers for stable walking of an underactuated 3D bipedal robot with point feet and 13 DOFs [35, 36, 38]. The video of our experiments is available online [39]. Reference [37] also extended the algorithm to design robust optimal controllers for hybrid models of bipedal running. Our approach is mainly based on optimization techniques and matrix inequalities in the *full-order state space*. Roughly speaking by employing a family of nonlinear controllers parameterized by ξ, the evolution of the hybrid system on a Poincaré section $\mathcal{S}$ can be described by a parameterized Poincaré map given by

$$x[k+1] = P\left(x[k], \xi\right), \quad k = 0, 1, \cdots \tag{1}$$

whose fixed point $x^\star$ is assumed to be invariant under the choice of the controller parameters ξ. When following the Poincaré analysis, the exponential stabilization problem of the corresponding periodic orbit consists of finding ξ such that the following matrix inequality

$$\mathcal{I}\left(A(\xi), W, \gamma\right) := \begin{bmatrix} W & A(\xi)\, W \\ \star & (1-\gamma)\, W \end{bmatrix} > 0, \tag{2}$$

is satisfied, in which $A(\xi) \in \mathbb{R}^{(n-1)\times(n-1)}$ represents the Jacobian linearization of the Poincaré map with respect to x, evaluated at the fixed point $x^\star$, n is the order of the hybrid system, $W = W^\top > 0$ is a Lyapunov matrix, and $\gamma > 0$ denotes a scalar to tune the convergence rate. To look for a set of controller parameters ξ, we then set up an optimization problem as follows [35, 36, 37, 40]

$$\min_{(\xi, W, \gamma)} \mathcal{J}\left(\xi, \gamma\right) \tag{3}$$

$$\text{s.t. } \mathcal{I}\left(A(\xi), W, \gamma\right) > 0 \tag{4}$$

for some smooth cost function $\mathcal{J}(.,.)$. We see that the Lyapunov matrix W contains $\frac{n(n-1)}{2}$ scalar entries. The optimization problem (3) and (4) requires $p + \frac{n(n-1)}{2} + 1$ decision variables, where p represents the dimension of the controller parameters ξ. When n is significantly large, the number of the resulting Lyapunov variables becomes dominant and the optimization problem may be computationally prohibitive. In order to reduce the number of decision variables in the optimization framework, we are interested in applying a change of coordinates in the state space as follows

$$\hat{x} := \begin{bmatrix} z \\ \eta \end{bmatrix} := \Psi(x, \xi) \tag{5}$$

to translate the optimization problem (3) and (4) into an equivalent one in terms of a *reduced-order* Jacobian and *lower-dimensional* Lyapunov matrices in the z-coordinates. This important numerical benefit of the coordinate transform (5) also introduces an analytical challenge because the image of the Poincaré section itself may now depend on the parameters, viz $\hat{\mathcal{S}}_\xi := T(\mathcal{S}, \xi)$, whereas previously the "state space" of the Poincaré map was independent of the controller parameters.

The contribution of this paper is to present a systematic framework based on the concept of hybrid invariant manifolds to reduce the number of decision variables in (3) and (4). The framework assumes a family of parameterized output functions to be regulated for the continuous-time portion of the hybrid system using input-output (I-O) linearizing controllers [41]. It also assumes a family of parameterized event-based controllers. We remark that these event-based laws are *not* utilized to stabilize orbits. They are instead employed to make the corresponding parameterized zero dynamics manifolds hybrid invariant under the reset map of the hybrid system. The paper then investigates the structure of the parameterized Poincaré map. It presents a systematic numerical approach to compute the Jacobian linearization of the Poincaré map and then develops a reduced-order stability analysis on a parameterized family of Poincaré sections. To illustrate the power of the framework, it is finally applied to exponentially stabilize walking gaits of an underactuated 3D bipedal robot with 13 DOFs. It is shown that the number of decision variables in the reduced-order framework can be decreased by 70% compared to the optimization problem employed in [35].

For dynamical systems with hybrid invariant manifolds, [42] presented a local coordinate transform under which the Jacobian linearization of the

Poincaré map has a block upper triangular structure. It also provided conditions under which the exponential stabilization problem of periodic orbits for the full-order models can be translated to a reduced-order model based on restricted Poincaré maps on the hybrid invariant manifolds. As alluded to earlier, when the controller parameters intervene in the Poincaré sections and hybrid invariant manifolds, the analysis of the restricted Poincaré maps is more subtle. In particular, reference [42] did *not* investigate the stabilization problem for a family of parameterized manifolds. In addition, it did *not* consider the effect of output parameters as well as event-based update laws on the Jacobian linearization of the Poincaré map. The current paper first addresses these issues and subsequently presents a systematic numerical approach to compute parameterized restricted Poincaré maps for a reduced-order framework.

The paper is organized as follows. Section 2 presents open-loop hybrid models. It develops family of parameterized I-O linearizing controllers and event-based control laws. The properties of closed-loop hybrid systems and Poincaré return map are also investigated in Section 2. Section 3 presents a computational approach for the Jacobian linearization and reduced-order stabilization framework. Section 4 extends the analytical results to the hybrid models of bipedal walking and illustrates the method by determining stabilizing controllers for an underactuated bipedal robot. Section 5 contains concluding remarks.

2. Hybrid Model

We consider single-phase hybrid dynamical systems of a form that naturally arises in bipedal walking as follows

$$\Sigma : \begin{cases} \dot{x} = f(x) + g(x)\, u, & x^- \notin \mathcal{S} \\ x^+ = \Delta(x^-), & x^- \in \mathcal{S}, \end{cases} \tag{6}$$

in which $x \in \mathcal{X}$ and $u \in \mathcal{U}$ represent the *state variables* and *continuous-time control inputs*, respectively. The *state manifold* and *set of admissible control inputs* are denoted by $\mathcal{X} \subset \mathbb{R}^n$ and $\mathcal{U} \subset \mathbb{R}^m$ for some positive integers n and m. The continuous-time portion of the hybrid system is represented by the ordinary differential equation (ODE) $\dot{x} = f(x)+g(x)\, u$, where the vector field $f : \mathcal{X} \to \mathsf{T}\mathcal{X}$ and columns of g (i.e., $g_j(x)$ for $j = 1, \cdots, m$) are assumed to be smooth (i.e., $\mathcal{C}^\infty$). $\mathsf{T}\mathcal{X}$ denotes the tangent bundle of the state manifold $\mathcal{X}$.

We further suppose that the distribution generated by the columns of $g(x)$, i.e., $\Omega(x) := \text{span}\{g_1(x), \cdots, g_m(x)\}$, is involutive. The discrete-time portion of the hybrid system is also represented by $x^+ = \Delta(x^-)$, where $\Delta : \mathcal{X} \to \mathcal{X}$ is a $\mathcal{C}^\infty$ *reset map*, and $x^-(t) := \lim_{\tau \nearrow t} x(\tau)$ and $x^+(t) := \lim_{\tau \searrow t} x(\tau)$ denote the left and right limits of the state trajectory $x(t)$, respectively. The guard of the hybrid system is then given by the *switching manifold*

$$\mathcal{S} := \{x \in \mathcal{X} \mid s(x) = 0, \sigma(x) < 0\} \tag{7}$$

on which the state solutions of the hybrid system (6) undergo an abrupt change according to the reset map. Furthermore, $s : \mathcal{X} \to \mathbb{R}$ represents a $\mathcal{C}^\infty$ *switching function* with the property $\frac{\partial s}{\partial x}(x) \neq 0$ for all $x \in \mathcal{S}$. Finally, $\sigma : \mathcal{X} \to \mathbb{R}$ denotes a $\mathcal{C}^\infty$ function to determine feasible switching events as $\sigma(x) < 0$. The solutions of the hybrid system (6) are constructed by piecing together the flows of the continuous-time phase such that the re-initialization rule $x^+ = \Delta(x^-)$ is applied when the flows intersect the switching manifold $\mathcal{S}$. Throughout this paper, we shall assume that the solutions of (6) are right-continuous. We further suppose that there exists a period-one orbit $\mathcal{O}$ for (6) which is transversal to the switching manifold $\mathcal{S}$. The precise assumptions are as follows.

Assumption 1 (Transversal Period-One Orbit)**.** There exist a bounded period $T^\star > 0$ (referred to as the *fundamental period*), smooth *nominal control input* $u^\star : [0, T^\star] \to \mathcal{U}$, and a smooth *nominal state solution* $\varphi^\star : [0, T^\star] \to \mathcal{X}$ such that the following conditions are satisfied:

1. $\dot{\varphi}^\star(t) = f(\varphi^\star(t)) + g(\varphi^\star(t))\, u^\star(t)$ for all $t \in [0, T^\star]$;
2. $\varphi^\star(t) \notin \mathcal{S}$ for all $t \in [0, T^\star)$ and $\varphi^\star(T^\star) \in \mathcal{S}$;
3. $\varphi^\star(0) = \Delta(\varphi^\star(T^\star))$ (periodicity condition); and
4. $\dot{s}(\varphi^\star(T^\star)) = \frac{\partial s}{\partial x}(\varphi^\star(T^\star))\, \dot{\varphi}^\star(T^\star) \neq 0$ (transversality condition).

Then,

$$\mathcal{O} := \{x = \varphi^\star(t) \mid 0 \leq t < T^\star\} \tag{8}$$

is a *period-one orbit* for the hybrid system (6) which is *transversal* to the switching manifold $\mathcal{S}$. In addition,

$$\{x^\star\} := \overline{\mathcal{O}} \cap \mathcal{S} = \{\varphi^\star(T^\star)\} \tag{9}$$

is a singleton, in which $\overline{\mathcal{O}}$ denotes the set closure of the orbit $\mathcal{O}$.

Throughout this paper, we shall consider $\mathcal{O}$ as the *desired periodic orbit* to be stabilized and we will assume that there is a smooth and real-valued function, referred to as the *phasing variable*, which is strictly increasing along $\mathcal{O}$. The phasing variable replaces time which is a key to obtaining *time-invariant* feedback controllers to exponentially stabilize the periodic orbit. In particular, it represents the progress of the system (e.g., robot) on the periodic orbit (e.g., walking gait). The precise conditions are as follows.

Assumption 2 (Phasing Variable)**.** There exists a smooth function $\theta : \mathcal{X} \to \mathbb{R}$ such that $\mathrm{L}_{g_j}\theta(x) = 0$ for all $x \in \mathcal{X}$ and $j = 1, \cdots, m$. Furthermore, $\theta(x)$ is strictly increasing on the orbit $\mathcal{O}$. In particular, there is an open neighborhood of $\mathcal{O}$, denoted by $\mathcal{N}(\mathcal{O}) \subset \mathcal{X}$, such that for every $x \in \mathcal{N}(\mathcal{O})$, $\dot{\theta}(x) = \mathrm{L}_f\theta(x) > 0$.

Reference [23] shows that the existence of a phasing variable follows directly from Assumption 1 on the periodic orbit.

2.1. Family of Parameterized I-O Linearizing Controllers

In order to exponentially stabilize the periodic orbit $\mathcal{O}$, we consider a *parameterized family of output functions*, to be regulated for the continuous-time portion of the hybrid system, as follows

$$y := h\left(x, \xi, \alpha\right) := \begin{cases} \mathrm{fcn}\left(x, \xi, \alpha\right), & \text{if } \theta(x) \leq \theta_{\mathrm{th}} \\ \mathrm{fcn}\left(x, \xi, \alpha^{\star}\right), & \text{otherwise,} \end{cases} \tag{10}$$

in which $\dim(y) = \dim(u) = m$. The family of output functions in (10) is defined in a piece-wise manner for which $\theta(x) = \theta_{\mathrm{th}}$, a level set of the phasing variable, determines the sub-domains in (10). Here $\theta_{\mathrm{th}} \in (\theta_{\mathrm{min}}, \theta_{\mathrm{max}})$ denotes a threshold value, where θ_{min} and θ_{max} represent the limits of the phasing variable on $\overline{\mathcal{O}}$, i.e., $\theta_{\mathrm{min}} := \min_{x \in \overline{\mathcal{O}}} \theta(x)$ and $\theta_{\mathrm{max}} := \max_{x \in \overline{\mathcal{O}}} \theta(x)$. In addition, the sub-function $\mathrm{fcn} : \mathcal{X} \times \Xi \times \mathcal{A} \to \mathbb{R}^m$ is parameterized by two sets of parameters ξ and α. The first set includes the *continuous-time parameters* $\xi \in \Xi \subset \mathbb{R}^{p_c}$, whereas the second set includes the *discrete-time parameters* $\alpha \in \mathcal{A} \subset \mathbb{R}^{p_d}$ for some connected and open sets Ξ and $\mathcal{A}$ and some positive integers p_c and p_d. In addition, $\alpha^{\star} \in \mathcal{A}$ represents a *nominal discrete-time parameter* based on which the sub-functions in (10) (i.e., for $\theta \leq \theta_{\mathrm{th}}$ and $\theta > \theta_{\mathrm{th}}$) are differentiated.

Roles of the Output Parameters: In this stabilization strategy, the parameters ξ are identically constant. They will be selected by offline optimization

with cost (3) and constraints (4) to render the fixed-point of a Poincaré map locally exponentially stable. The parameters α, referred to as the *event-based parameters*, will be kept constant during the continuous-time phase. However, they are allowed to be updated by an *event-based update law* when state trajectories intersect the switching manifold $\mathcal{S}$ to generate a family of *hybrid invariant* manifolds in the state space that will ultimately reduce the number of decision variables in the optimization problem (3) and (4). In what follows, we will set up a required set of assumptions to follow this strategy.

Assumption 3 (Uniform Relative Degree)**.** The family of parameterized outputs in (10) fulfills the following conditions.

1. h is at least w-times differentiable with respect to (x, ξ) on $\mathcal{N}(\mathcal{O}) \times \Xi$ for every $\alpha \in \mathcal{A}$ and some $w \geq 2$.
2. The sub-function fcn is at least w-times differentiable with respect to α on $\mathcal{A}$ for every $(x, \xi) \in \mathcal{N}(\mathcal{O}) \times \Xi$.
3. The output function $h(x, \xi, \alpha)$ has uniform relative degree $r < w$ with respect to u on $\mathcal{N}(\mathcal{O}) \times \Xi \times \mathcal{A}$. That is,

$$\mathrm{L}_{g_j}\mathrm{L}_f^i h\,(x, \xi, \alpha) = 0, \text{ and } \det\left(\mathrm{L}_g\mathrm{L}_f^{r-1} h\,(x, \xi, \alpha)\right) \neq 0,$$

   for all $(x, \xi, \alpha) \in \mathcal{N}(\mathcal{O}) \times \Xi \times \mathcal{A}$, $i = 0, 1, \cdots, r-2$, and $j = 1, \cdots, m$.
4. For every $(\xi, \alpha) \in \Xi \times \mathcal{A}$,

$$\mathcal{Z}(\xi, \alpha) := \{x \in \mathcal{X} \,|\, h(x, \xi, \alpha) = \mathrm{L}_f h(x, \xi, \alpha) = \cdots = \mathrm{L}_f^{r-1} h(x, \xi, \alpha) = 0\} \tag{11}$$

   is a nonempty set.
5. $h(x, \xi, \alpha^\star)$ is identically zero on the periodic orbit for every $\xi \in \Xi$, i.e., $h\,(x, \xi, \alpha^\star) = 0$ for all $(x, \xi) \in \overline{\mathcal{O}} \times \Xi$.

Assumption 3 presents the family of *parameterized zero dynamics manifolds* (11) on which the output function h is identically zero. From Items 3 and 4 of Assumption 3, each member of this family is a $k := n - rm$ dimensional embedded sub-manifold of $\mathcal{X}$. Furthermore, Item 5 of Assumption 3 implies that $\mathcal{O}$ is an *invariant subset* for the family of zero dynamics manifolds $\mathcal{Z}(\xi, \alpha^\star)$ for all values of ξ, i.e., $\mathcal{O} \subset \mathcal{Z}\,(\xi, \alpha^\star)$ for all $\xi \in \Xi$ (see Fig. 1.a). This will help us to look for continuous-time parameters ξ without changing the desired orbit. In order to clarify the idea, the following example presents a family of parameterized output functions that satisfy Items 1, 2, and 5 of Assumption 3.

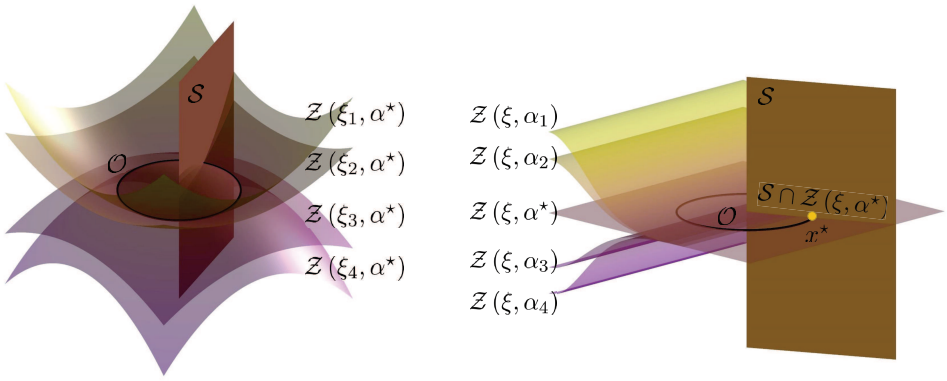

(a) (b)

Figure 1: (a) Geometric illustration of the periodic orbit $\mathcal{O}$ and family of zero dynamics manifolds $\mathcal{Z}(\xi, \alpha^\star)$ for four different continuous-time parameters $\xi_1, \xi_2, \xi_3, \xi_4 \in \Xi$. Here $\alpha = \alpha^\star$ is fixed and from Item 5 of Assumption 3, $\mathcal{O} \subset \mathcal{Z}(\xi, \alpha^\star)$ for every $\xi \in \Xi$. (b) Geometric description of the family of zero dynamics manifolds $\mathcal{Z}(\xi, \alpha)$ for four different discrete-time parameters $\alpha_1, \alpha_2, \alpha_3, \alpha_4 \in \mathcal{A}$ and a fixed $\xi \in \Xi$. According to the construction procedure in Assumption 5, $\mathcal{S} \cap \mathcal{Z}(\xi, \alpha) = \mathcal{S} \cap \mathcal{Z}(\xi, \alpha^\star)$ for every $\xi \in \Xi$ and $\alpha \in \mathcal{A}$.

Example 1. This example illustrates a parameterization of output functions for which the outputs are constructed by adding nominal and corrective portions as follows

$$h(x, \xi, \alpha) = \underbrace{H(\xi)\left(x - x_{\mathrm{d}}\left(\theta(x)\right)\right)}_{=: h_{\mathrm{nom}}(x, \xi)} - h_{\mathrm{corr}}\left(\theta(x), \alpha\right), \tag{12}$$

where $x_{\mathrm{d}}(\theta)$ represents the desired evolution of the state variables on $\mathcal{O}$ in terms of the phasing variable $\theta(x)$. In particular,

$$x_{\mathrm{d}}\left(\theta\right) := \varphi^\star(t)\,\big|_{t = \boldsymbol{\theta}^{-1}(\theta)}\,, \tag{13}$$

in which $\varphi^\star(t)$ was already defined in Assumption 1, and $\theta = \boldsymbol{\theta}(t)$ and $t = \boldsymbol{\theta}^{-1}(\theta)$ denote the evolution of the phasing variable on $\mathcal{O}$ and its inverse function, respectively. In (12), $h_{\mathrm{nom}}(x, \xi) \in \mathbb{R}^m$ also denotes a *nominal output function* vanishing on the orbit $\mathcal{O}$, and $H(\xi) \in \mathbb{R}^{m \times n}$ represents a parameterized *output matrix* to be determined. One can assume that ξ denotes the columns of the H matrix, i.e., $\xi = \mathrm{vec}(H)$, where vec(.) is the

vectorization operator. The *corrective term* is then defined as

$$h_{\text{corr}}(\theta,\alpha) := \begin{cases} b(\theta,\alpha), & \text{if } \theta \leq \theta_{\text{th}} \\ b(\theta,\alpha^\star), & \text{otherwise} \end{cases} \tag{14}$$

to zero the output function (12) right after the switching event (this will be clarified with more details in Section 2.2). To satisfy Items 1, 2, and 5 of Assumption 3, the function $b : \mathbb{R} \times \mathcal{A} \to \mathbb{R}^m$ is finally assumed to be w-times differentiable with respect to (θ, α) with the following properties:

1. $b(\theta, \alpha^\star) \equiv 0$ for some $\alpha^\star \in \mathcal{A}$.
2. $b(\theta_{\text{th}}, \alpha) = \frac{\partial b}{\partial \theta}(\theta_{\text{th}}, \alpha) = \cdots = \frac{\partial^w b}{\partial \theta^w}(\theta_{\text{th}}, \alpha) = 0$ for every $\alpha \in \mathcal{A}$.

Using these properties, one can easily see that Item 5 of Assumption 3 is satisfied. Furthermore, these properties make the piece-wise defined corrective function in (14) w-times differentiable with respect to θ which in combination with Assumption 2 fulfills Item 1 of Assumption 3.

Now we are in a position to present a diffeomorphism to investigate the evolution of the hybrid system in a set of tangent and transverse coordinates. The following assumption presents a valid change of coordinates for the state space in which the tangent coordinates for the family of zero dynamics manifolds in (11) are assumed to be *independent* of the value of the continuous- and discrete-time parameters ξ and α.

Assumption 4 (Invariant Tangent Coordinates)**.** There exists a smooth function $z : \mathcal{X} \to \mathbb{R}^k$, referred to as the *tangent coordinates*, with the property $\mathrm{L}_{g_j} z(x) = 0$ for all $j = 1, \cdots, m$ such that the mapping $\Psi : \mathcal{X} \times \Xi \times \mathcal{A} \to \mathbb{R}^n$ by

$$\hat{x} = \Psi(x, \xi, \alpha) := \begin{bmatrix} z(x) \\ \eta(x, \xi, \alpha) \end{bmatrix} \tag{15}$$

is a diffeomorphism to its image, where

$$\eta(x, \xi, \alpha) := \begin{bmatrix} h(x, \xi, \alpha) \\ \mathrm{L}_f h(x, \xi, \alpha) \\ \vdots \\ \mathrm{L}_f^{r-1} h(x, \xi, \alpha) \end{bmatrix} \in \mathbb{R}^{rm}. \tag{16}$$

denotes the *transverse coordinates*.

From the relative degree condition in Item 3 of Assumption 3, one can present a valid change of coordinates, parameterized by (ξ, α), to represent the continuous-time portion of the hybrid system in a set of tangent and transverse coordinates [41, Proposition 5.1.2]. However, Assumption 4 presents a *special structure* for the corresponding diffeomorphism by supposing that the tangent coordinates $z(x)$ are independent of the value of the output parameters (ξ, α). The motivation for this assumption comes from a set of coordinates introduced in [26, Appendix A] to describe zero dynamics of underactuated robots. This will help us to simplify the computation of the parameterized Poincaré map and the stability analysis in Sections 2.3 and 3. An example of a set of tangent coordinates satisfying this assumption will also be presented for the numerical results of Section 4. We remark that the transverse coordinates $\eta(x, \xi, \alpha)$ in Assumption 4 are free to be parameterized by the output parameters.

In order to make the family of zero dynamics manifolds $\mathcal{Z}(\xi, \alpha)$ *attractive* and *forward invariant* under the flow of the closed-loop continuous-time phase, we now employ a family of parameterized nonlinear controllers, arising from the standard I-O linearization technique [41], as follows

$$\Gamma(x, \xi, \alpha) := -\left(\mathrm{L}_g \mathrm{L}_f^{r-1} h(x, \xi, \alpha)\right)^{-1} \left(\mathrm{L}_f^r h(x, \xi, \alpha) + \sum_{j=0}^{r-1} \frac{k_j}{\varepsilon^{r-j}} \mathrm{L}_f^j h(x, \xi, \alpha)\right), \tag{17}$$

where $\varepsilon > 0$ and the constants k_j for $j = 0, 1, \cdots, r-1$ are chosen such that the monic polynomial $\chi(\lambda) := \lambda^r + k_{r-1}\lambda^{r-1} + \cdots + k_0$ becomes Hurwitz. Applying the feedback law (17) results in the *output dynamics*

$$y^{(r)} + \frac{k_{r-1}}{\varepsilon} y^{(r-1)} + \cdots + \frac{k_0}{\varepsilon^r} y = 0 \tag{18}$$

for which the origin is exponentially stable[1]. In addition, the output dynamics (18) can be written in the following compact equation

$$\dot{\eta} = F(\varepsilon)\, \eta \tag{19}$$

[1]For every $\varepsilon > 0$, $\bar{\lambda}$ is a root for $\chi(\lambda) = 0$ if and only if $\frac{1}{\varepsilon}\bar{\lambda}$ becomes a root for $\chi(\lambda, \varepsilon) = \lambda^r + \frac{k_{r-1}}{\varepsilon}\lambda^{r-1} + \cdots + \frac{k_0}{\varepsilon^r} = 0$. Therefore, $\chi(\lambda)$ is a Hurwitz polynomial if and only if $\chi(\lambda, \varepsilon)$ is Hurwitz.

in which $F(\varepsilon) \in \mathbb{R}^{rm \times rm}$ is a Hurwitz matrix with the property $\lim_{\varepsilon \searrow 0} \exp(F(\varepsilon)\, T^\star) = 0$ [42]. The *tangent dynamics* can then be given by

$$\dot{z} = f_0\left(z, \eta, \xi, \alpha\right), \tag{20}$$

where

$$\begin{bmatrix} f_0\left(z, \eta, \xi, \alpha\right) \\ F(\varepsilon)\, \eta \end{bmatrix} = \frac{\partial \Psi}{\partial x}\left(x, \xi, \alpha\right)\, f^{\mathrm{cl}}\left(x, \xi, \alpha\right)\Big|_{x=\Psi^{-1}(z,\eta,\xi,\alpha)}$$

and $f^{\mathrm{cl}}(x, \xi, \alpha) := f(x) + g(x)\, \Gamma(x, \xi, \alpha)$ and $\Psi^{-1}(z, \eta, \xi, \alpha)$ represent the closed-loop vector field and inverse of the mapping (15), respectively. The superscript "cl" also stands for the closed-loop system. For later purposes, the family of the zero dynamics manifolds (11) can be rewritten as $\mathcal{Z}(\xi, \alpha) = \{(z^\top, \eta^\top)^\top \,|\, \eta = 0\}$ for which the *parameterized zero dynamics* become

$$\dot{z} = f_0(z, 0, \xi, \alpha). \tag{21}$$

2.2. Hybrid Invariance

This section investigates the hybrid invariance property of the parameterized zero dynamics manifolds $\mathcal{Z}(\xi, \alpha)$. In particular, we present a set of parameterized event-based update laws to make the family of zero dynamics manifolds hybrid invariant under the flow of the closed-loop hybrid system. For this purpose from Assumption 2, $\theta(x)$ is strictly increasing on $\mathcal{O}$. According to the construction procedure of the output functions in (10) and the fact that $\theta_{\mathrm{th}} \in (\theta_{\min}, \theta_{\max})$, one can conclude that the periodic orbit $\mathcal{O}$ intersects the switching manifold $\mathcal{S}$ in the sub-domain $\theta(x) > \theta_{\mathrm{th}}$, i.e., $\theta(x^\star) > \theta_{\mathrm{th}}$. Thus, there is an open neighborhood $\mathcal{B}(x^\star) \subset \mathcal{N}(\mathcal{O})$ of $x^\star$ such that for every $(x, \xi, \alpha) \in \mathcal{B}(x^\star) \times \Xi \times \mathcal{A}$, $\theta(x) > \theta_{\mathrm{th}}$, and consequently, $h(x, \xi, \alpha) = h(x, \xi, \alpha^\star)$ (see the structure of the output function in (10)). This implies that for every $(x, \xi, \alpha) \in \mathcal{B}(x^\star) \times \Xi \times \mathcal{A}$, $x \in \mathcal{Z}(\xi, \alpha)$ if and only if $x \in \mathcal{Z}(\xi, \alpha^\star)$ (see Fig. 1.b). Now we are in a position to present the hybrid invariance assumption for the family of zero dynamics manifolds.

Assumption 5 (Hybrid Invariance)**.** We assume that for every fixed $\xi \in \Xi$, the family of zero dynamics manifolds $\mathcal{Z}(\xi, \alpha)$ has a *nonempty* and $k-1$ dimensional intersection with the switching manifold $\mathcal{S}$, shown by $\mathcal{S} \cap \mathcal{Z}(\xi, \alpha^\star)$, which is *independent* of the value of the discrete-time parameters α. That is,

$$\mathcal{S} \cap \mathcal{Z}\left(\xi, \alpha\right) = \mathcal{S} \cap \mathcal{Z}(\xi, \alpha^\star) \neq \emptyset, \quad \forall \alpha \in \mathcal{A} \tag{22}$$

(see again Fig. 1.b). We further suppose that the *hybrid invariance* property is satisfied. In particular, there exists a smooth and parameterized *event-based update law*[2] $v(z,\xi) \in \mathcal{A}$ such that (1) it maps $x^\star$ to $\alpha^\star$ for every $\xi \in \Xi$, i.e.,

$$v\left(z\left(x^\star\right),\xi\right) = \alpha^\star, \quad \forall \xi \in \Xi, \tag{23}$$

and (2) for all $x^- \in \mathcal{S} \cap \mathcal{Z}(\xi,\alpha^\star)$ and $\xi \in \Xi$,

$$x^+ \in \mathcal{Z}\left(\xi,\alpha^+\right), \tag{24}$$

where $x^+ = \Delta(x^-)$ and

$$\alpha^+ = v\left(z\left(x^-\right),\xi\right). \tag{25}$$

Remark 1. Assumption 5 has important consequences. First, the diffeomorphism Ψ, restricted to $\mathcal{B}(x^\star)$, becomes independent of the discrete-time parameters α and can be shown by $\Psi(x,\xi,\alpha^\star)$. This results in the following *local* image of the switching manifold $\mathcal{S}$ under the mapping $\Psi(x,\xi,\alpha^\star)$,

$$\hat{\mathcal{S}}_\xi := \left\{(z^\top,\eta^\top)^\top \mid \hat{s}\left(z,\eta,\xi\right) = 0\right\}, \tag{26}$$

where $\hat{s}(z,\eta,\xi) := s \circ \Psi^{-1}(z,\eta,\xi,\alpha^\star)$. Second, the reset map Δ can locally be expressed in the (z,η) coordinates as follows

$$\begin{aligned}\hat{\Delta}\left(z^-,\eta^-,\xi\right) &:= \begin{bmatrix}\hat{\Delta}_z\left(z^-,\eta^-,\xi\right)\\ \hat{\Delta}_\eta\left(z^-,\eta^-,\xi\right)\end{bmatrix}\\ &:= \Psi\left(\Delta\left(x^-\right),\xi,\alpha^+\right)\Big|_{x^- = \Psi^{-1}\left(z^-,\eta^-,\xi,\alpha^\star\right),\, \alpha^+ = v\left(z^-,\xi\right)}\end{aligned} \tag{27}$$

in which the subscripts "z" and "η" stand for the z and η coordinates, respectively. For later purposes, we remark that $\hat{\mathcal{S}}_\xi$ and $\hat{\Delta}(z^-,\eta^-,\xi)$ are *only* parameterized by the continuous-time parameters ξ which will affect the structure of the Jacobian matrix of the Poincaré map in Theorem 1.

2.3. Closed-Loop Hybrid Model and Poincaré Return Map

By employing the I-O linearizing controller (17) and the event-based update law (25), the closed-loop hybrid model becomes

$$\Sigma^{\mathrm{cl}}: \begin{cases} \begin{bmatrix}\dot{x}\\ \dot{\alpha}\end{bmatrix} = \begin{bmatrix}f^{\mathrm{cl}}(x,\xi,\alpha)\\ 0\end{bmatrix}, & x^- \notin \mathcal{S}\\ \begin{bmatrix}x^+\\ \alpha^+\end{bmatrix} = \begin{bmatrix}\Delta\left(x^-\right)\\ v\left(z\left(x^-\right),\xi\right)\end{bmatrix}, & x^- \in \mathcal{S},\end{cases} \tag{28}$$

[2]The event-based update law is only parameterized by the continuous-time parameters.

where the discrete-time parameters α are kept constant during the continuous-time phase, i.e., $\dot{\alpha} = 0$ and are updated according to the event-based law $\alpha^+ = v(z(x^-), \xi)$ on the switching manifold $\mathcal{S}$. Here, the continuous-time parameters ξ are assumed to be constant.

Lemma 1 (Invariant Periodic Orbit)**.** Assume that Assumptions 1-5 are satisfied. Then, $\mathcal{O} \times \{\alpha^\star\}$ is a period-one orbit for (28) which is transversal to $\mathcal{S} \times \mathcal{A}$. Furthermore, this orbit is independent of the value of the continuous-time parameters ξ.

Proof. According to the construction procedure in Item 5 of Assumption 3, $\mathcal{O} \subset \mathcal{Z}(\xi, \alpha^\star)$ for all $\xi \in \Xi$. In addition from Item 3 of Assumption 3, the decoupling matrix is square and full rank, and the control driving $h(x, \xi, \alpha^\star)$ to zero is unique on $\mathcal{Z}(\xi, \alpha^\star)$ [41, pp. 226]. Hence, the control $\Gamma(x, \xi, \alpha^\star)$, restricted to $\overline{\mathcal{O}}$, becomes independent of ξ. This fact together with Assumption 4 and (23) implies that $\mathcal{O} \times \{\alpha^\star\}$ is an orbit of (28) for all $\xi \in \Xi$. Transversality follows directly from Assumption 1. □

For later purposes, the unique solution of the parameterized ODE $\dot{x} = f^{\mathrm{cl}}(x, \xi, \alpha)$ (supposed to be at least $\mathcal{C}^1$) with the initial condition $x(0) = x_0$ is denoted by $\varphi(t, x_0, \xi, \alpha)$ for all $t \geq 0$ in the maximal interval of existence. The *time-to-switching function* $T : \mathcal{X} \times \Xi \times \mathcal{A} \to \mathbb{R}_{>0}$ is also defined as the first time at which the flow of the ODE intersects the switching manifold $\mathcal{S}$, that is,

$$T(x_0, \xi, \alpha) := \inf \{t > 0 \,|\, \varphi(t, x_0, \xi, \alpha) \in \mathcal{S}\}.$$

The evolution of the closed-loop hybrid system (28) on the Poincaré section $\mathcal{S} \times \mathcal{A}$ can then be described by the following discrete-time system

$$\begin{bmatrix} x[k+1] \\ \alpha[k+1] \end{bmatrix} = \begin{bmatrix} P(x[k], v(z(x[k]), \xi), \xi) \\ v(z(x[k]), \xi) \end{bmatrix}, \quad k = 0, 1, \cdots, \tag{29}$$

in which $P : \mathcal{S} \times \mathcal{A} \times \Xi \to \mathcal{S}$ by

$$P(x, \alpha, \xi) := \varphi(T(\Delta(x), \xi, \alpha), \Delta(x), \xi, \alpha) \tag{30}$$

denotes the *parameterized Poincaré map*. According to the construction procedure in Assumptions 3 and 4, and (23), $(x^\star, \alpha^\star)$ is an *invariant fixed point* for the discrete-time system (29) under the change of the continuous-time parameters ξ, i.e.,

$$\begin{bmatrix} P(x^\star, \alpha^\star, \xi) \\ v(z(x^\star), \xi) \end{bmatrix} = \begin{bmatrix} x^\star \\ \alpha^\star \end{bmatrix}, \quad \forall \xi \in \Xi. \tag{31}$$

In order to reduce the dimension of the stabilization problem, we now consider the discrete-time system (29) in the (z, η, α) coordinates as follows

$$\begin{bmatrix} z[k+1] \\ \eta[k+1] \\ \alpha[k+1] \end{bmatrix} = \begin{bmatrix} \hat{P}_z\left(z[k], \eta[k], v\left(z[k], \xi\right), \xi\right) \\ \hat{P}_\eta\left(z[k], \eta[k], v\left(z[k], \xi\right), \xi\right) \\ v\left(z[k], \xi\right) \end{bmatrix}, \tag{32}$$

where $\hat{P}(.,.,.,\xi) : \hat{\mathcal{S}}_\xi \times \mathcal{A} \to \hat{\mathcal{S}}_\xi$ is defined by[3]

$$\begin{aligned} \hat{P}\left(z, \eta, \alpha, \xi\right) &:= \begin{bmatrix} \hat{P}_z\left(z, \eta, \alpha, \xi\right) \\ \hat{P}_\eta\left(z, \eta, \alpha, \xi\right) \end{bmatrix} \\ &:= \Psi\left(P\left(\Psi^{-1}\left(z, \eta, \xi, \alpha^\star\right), \alpha, \xi\right), \xi, \alpha^\star\right). \end{aligned} \tag{33}$$

Direct calculations shows that (32) is a Poincaré map for the following hybrid system

$$\hat{\Sigma}^{\text{cl}} : \begin{cases} \begin{bmatrix} \dot{z} \\ \dot{\eta} \\ \dot{\alpha} \end{bmatrix} = \begin{bmatrix} f_0\left(z, \eta, \xi, \alpha\right) \\ F(\varepsilon)\,\eta \\ 0 \end{bmatrix}, & \begin{bmatrix} z^- \\ \eta^- \end{bmatrix} \notin \hat{\mathcal{S}}_\xi \\ \begin{bmatrix} z^+ \\ \eta^+ \\ \alpha^+ \end{bmatrix} = \begin{bmatrix} \hat{\Delta}_z\left(z^-, \eta^-, \xi\right) \\ \hat{\Delta}_\eta\left(z^-, \eta^-, \xi\right) \\ v\left(z^-, \xi\right) \end{bmatrix}, & \begin{bmatrix} z^- \\ \eta^- \end{bmatrix} \in \hat{\mathcal{S}}_\xi, \end{cases} \tag{34}$$

for which the Poincaré section $\hat{\mathcal{S}}_\xi \times \mathcal{A}$ is parameterized by ξ. Now we are in a position to present the fundamental properties of the closed-loop hybrid model (34) based on which the main results will be presented in Section 3.

Lemma 2 (Properties of the Closed-Loop Hybrid System)**.** Under Assumptions 1-5, the following statements are correct.

1. *(Invariant Image of the Orbit):* The projection of the periodic orbit $\mathcal{O}$ under the mapping $\Psi(.,\xi,\alpha^\star)$ is independent of the value of the continuous-time parameters ξ and can be given by $\hat{\mathcal{O}} := \hat{\mathcal{O}}_z \times \{0\}$, where $\hat{\mathcal{O}}_z := \{z = \hat{\varphi}_z^\star(t) \,|\, t \in [0, T^\star)\}$ and

$$\begin{bmatrix} \hat{\varphi}_z^\star(t) \\ 0 \end{bmatrix} := \Psi\left(\varphi^\star(t), \xi, \alpha^\star\right), \ \forall (t, \xi) \in [0, T^\star] \times \Xi. \tag{35}$$

[3]In (33), we have made use of the assumption that Ψ and Ψ^{-1} on $\mathcal{B}(x^\star) \cap \mathcal{S}$ and $\hat{\mathcal{S}}_\xi$ do not change by the discrete-time parameters α, respectively (see Remark 1).

In particular, $(z^{\star\top}, 0)^\top := \Psi(x^\star, \xi, \alpha^\star)$ is independent of the choice of $\xi \in \Xi$.

2. *(Invariant Orbit):* For every $\xi \in \Xi$, $\hat{\mathcal{O}} \times \{\alpha^\star\}$ is a periodic orbit for (34) which is transversal to $\hat{\mathcal{S}}_\xi \times \mathcal{A}$. More specifically, the following independence properties are satisfied

$$\frac{\partial f_0}{\partial \xi}(\hat{\varphi}_z^\star(t), 0, \xi, \alpha^\star) = 0, \quad \forall (t, \xi) \in [0, T^\star] \times \Xi \tag{36}$$

$$\frac{\partial \hat{s}}{\partial \xi}(z^\star, 0, \xi) = 0, \qquad \forall \xi \in \Xi \tag{37}$$

$$\frac{\partial \hat{\Delta}_z}{\partial \xi}(z^\star, 0, \xi) = 0, \qquad \forall \xi \in \Xi \tag{38}$$

$$\frac{\partial \hat{\Delta}_\eta}{\partial \xi}(z^\star, 0, \xi) = 0, \qquad \forall \xi \in \Xi. \tag{39}$$

3. *(Hybrid Invariance):* $\hat{\Delta}_\eta(z^-, 0, \xi) = 0$ for all $\xi \in \Xi$ and z^- in an open neighborhood of $z^\star$.

Proof. Part (1): According to Item 5 of Assumption 3 and the construction procedure in (16), one can conclude that $\eta(x, \xi, \alpha^\star) = 0$ for all $(x, \xi) \in \overline{\mathcal{O}} \times \Xi$. In addition from Assumption 4, the tangent coordinates $z(x)$ are independent of the value of ξ. These two facts result in (35).

Part (2): From Lemma 1, $\mathcal{O} \times \{\alpha^\star\}$ is a transversal periodic orbit for (28) which is independent of the value of ξ. This in combination with Part (1) of Lemma 2 implies that $\hat{\mathcal{O}} \times \{\alpha^\star\}$ is also a transversal[4] orbit for (34). Equations (36)-(39) are immediate consequences of the invariance property with respect to ξ.

Part (3) follows directly from Assumption 5. □

3. Main Results

The objective of this section is to present a reduced-order exponential stabilization framework to systematically search for continuous-time parameters ξ. The state space for the discrete-time system (32) is taken as $\hat{\mathcal{S}}_\xi \times \mathcal{A}$ which is parameterized by ξ. This complicates the computation of the parameterized

[4]We remark that the transversality is invariant under the valid change of coordinates.

Poincaré map as well as the stabilization problem when one looks for a set of continuous-time parameters ξ using the optimization framework of (3) and (4). To address these problems, this section introduces an *augmented closed-loop hybrid system* whose Poincaré section is *not* parameterized by ξ. Next it presents a asystematic way to numerically compute the Jacobian of the corresponding parameterized Poincaré map. The resultant Jacobian matrix is finally investigated to present a reduced-order stabilization framework.

To achieve the goals of this section, let us consider the following augmented system in the (z, η, α, ξ) coordinates

$$\hat{\Sigma}_a^{\mathrm{cl}} : \begin{cases} \begin{bmatrix} \dot{z} \\ \dot{\eta} \\ \dot{\alpha} \\ \dot{\xi} \end{bmatrix} = \begin{bmatrix} f_0(z, \eta, \xi, \alpha) \\ F(\varepsilon)\, \eta \\ 0 \\ 0 \end{bmatrix}, & \begin{bmatrix} z^- \\ \eta^- \\ \alpha^- \\ \xi^- \end{bmatrix} \notin \hat{\mathcal{S}}_a \\ \begin{bmatrix} z^+ \\ \eta^+ \\ \alpha^+ \\ \xi^+ \end{bmatrix} = \begin{bmatrix} \hat{\Delta}_z\left(z^-, \eta^-, \xi^-\right) \\ \hat{\Delta}_\eta\left(z^-, \eta^-, \xi^-\right) \\ v\left(z^-, \xi^-\right) \\ \xi^- \end{bmatrix}, & \begin{bmatrix} z^- \\ \eta^- \\ \alpha^- \\ \xi^- \end{bmatrix} \in \hat{\mathcal{S}}_a, \end{cases} \tag{40}$$

where ξ is now taken as one of the state variables,

$$\hat{\mathcal{S}}_a := \left\{ (z^\top, \eta^\top, \alpha^\top, \xi^\top)^\top \mid \hat{s}\left(z, \eta, \xi\right) = 0 \right\} \tag{41}$$

denotes an *augmented switching manifold*, and the subscript "a" stands for the augmented system. In order to keep ξ constant, the evolution of ξ during the continuous- and discrete-time phases of the augmented model (40) is described by $\dot{\xi} = 0$ and $\xi^+ = \xi^-$, respectively. To study the stabilization problem of the periodic orbit $\mathcal{O}$ for the closed-loop hybrid system, we consider the *augmented Poincaré return map* for (40) which is defined as $\hat{P}_a : \hat{\mathcal{S}}_a \to \hat{\mathcal{S}}_a$ by

$$\hat{P}_a\left(z, \eta, \alpha, \xi\right) := \begin{bmatrix} \hat{P}_z\left(z, \eta, v\left(z, \xi\right), \xi\right) \\ \hat{P}_\eta\left(z, \eta, v\left(z, \xi\right), \xi\right) \\ v\left(z, \xi\right) \\ \xi \end{bmatrix}. \tag{42}$$

The following theorem addresses the properties of the augmented Poincaré map.

Theorem 1 (Properties of the Augmented Poincaré Map)**.** Assume that Assumptions 1-5 are satisfied. Then, the following statements are correct.

1. *(Augmented Orbit):* For every $\xi \in \Xi$, $\hat{\mathcal{O}}_a := \hat{\mathcal{O}}_z \times \{0\} \times \{\alpha^\star\} \times \{\xi\}$ is a periodic orbit for the augmented hybrid system (40). Furthermore, $\hat{\mathcal{O}}_a$ is transversal to $\hat{\mathcal{S}}_a$.
2. *(Augmented Fixed Point):* For every $\xi \in \Xi$, $(z^{\star\top}, 0, \alpha^{\star\top}, \xi^\top)^\top$ is a fixed point of $\hat{P}_a$, i.e., the fixed points are not isolated.
3. *(Structure of the Augmented Jacobian Matrix):* For every $\xi \in \Xi$, the Jacobian of the Poincaré map $\hat{P}_a$, evaluated at $(z^{\star\top}, 0, \alpha^{\star\top}, \xi^\top)^\top$, has the following structure

$$\left[\begin{array}{c|c|c|c} \mathrm{D}_z\hat{P}_z\left(z^\star, 0, \alpha^\star, \xi\right) & \mathrm{D}_\eta\hat{P}_z\left(z^\star, 0, \alpha^\star, \xi\right) & 0 & 0 \\ \hline 0 & \mathrm{D}_\eta\hat{P}_\eta\left(z^\star, 0, \alpha^\star, \xi\right) & 0 & 0 \\ \hline \mathrm{D}_z v(z^\star, \xi) & 0 & 0 & 0 \\ \hline 0 & 0 & 0 & I \end{array}\right]. \tag{43}$$

Remark 2 (Geometric Description)**.** According to the construction procedure in (40) and Parts (1) and (2) of Theorem 1, one can present a geometric description for the augmented orbit $\hat{O}_a$ in the state space of the system (40) (see Fig. 2). In this description, the augmented state space and augmented switching manifold for $\hat{\Sigma}_a$ are given by $\mathbb{R}^n \times \mathcal{A} \times \Xi$ and $\hat{S}_a$, respectively. When ξ changes, the family of augmented orbits can form a cylinder as $\hat{\mathcal{O}} \times \{\alpha^\star\} \times \Xi$. For a fixed $\xi \in \Xi$, the intersections of the augmented switching manifold $\hat{\mathcal{S}}_a$ and the cylinder with the hyperplane $\xi = \text{const}$ become $\hat{\mathcal{S}}_\xi$ and $\hat{\mathcal{O}} \times \{\alpha^\star\} \times \{\xi\}$, respectively. We remark that these intersections coincide with the switching manifold and periodic orbit of the closed-loop system $\hat{\Sigma}^{\mathrm{cl}}$ in (34). Item 3 of Theorem 1 presents a special structure for the Jacobian linearization of the augmented Poincaré map in (43) which will simplify the stabilization problem in Theorem 2. The problem of exponential stabilization consists of finding the continuous-time parameters ξ such that the intersection of the cylinder $\hat{\mathcal{O}} \times \{\alpha^\star\} \times \Xi$ with the hyperplane $\xi = \text{const}$ becomes exponentially stable for (34).

Proof. Parts (1) and (2) are immediate.

Part (3): Let us define the augmented state vector, closed-loop vector field, reset map, and switching function as $x_a := (z^\top, \eta^\top, \alpha^\top, \xi^\top)^\top$, $f_a(x_a) := (f_0^\top, \eta^\top F^\top, 0, 0)^\top$, $\Delta_a(x_a) := (\hat{\Delta}_z^\top, \hat{\Delta}_\eta^\top, v^\top, \xi^\top)^\top$, and $s_a(x_a) := \hat{s}$, respectively. In addition for a fixed $\xi \in \Xi$, the augmented nominal solution can be represented by $\varphi_a^\star(t) := (\hat{\varphi}_z^{\star\top}(t), 0, \alpha^{\star\top}, \xi^\top)^\top$ for every $t \in [0, T^\star]$. Next we define the Jacobian matrix of the augmented closed-loop vector field along

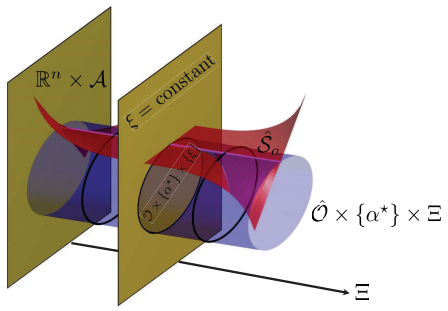

Figure 2: Geometric illustration of the augmented state space $\mathbb{R}^n \times \mathcal{A} \times \Xi$ and augmented switching manifold $\hat{S}_a$ for the closed-loop system $\hat{\Sigma}_a$ in (40). The figure depicts the cylinder $\hat{\mathcal{O}} \times \{\alpha^\star\} \times \Xi$ and a typical $\xi = \text{const}$ hyperplane.

$\hat{\mathcal{O}}_a$ as follows

$$A(t) := \frac{\partial f_a}{\partial x_a}(x_a)\,\big|_{x_a=\varphi_a^\star(t)}\,, \quad 0 \le t \le T^\star. \tag{44}$$

Suppose further $\Phi_a^\star(t)$ denotes the unique solution of the following matrix differential equation, referred to as the variational equation (VE) [22, Appendix B],

$$\begin{cases} \dot{\Phi}_a^\star(t) = A(t)\,\Phi_a^\star(t), \quad 0 \le t \le T^\star \\ \Phi_a^\star(0) = I. \end{cases} \tag{45}$$

From the structure of f_a and (36), one can conclude that

$$A(t) = \begin{bmatrix} A_{11}(t) & A_{12}(t) & A_{13}(t) & 0 \\ 0 & A_{22} & 0 & 0 \\ 0 & 0 & 0 & 0 \\ 0 & 0 & 0 & 0 \end{bmatrix}, \tag{46}$$

in which $A_{11}(t) := \frac{\partial f_0}{\partial z}(\hat{\varphi}_z^\star(t), 0, \xi, \alpha^\star)$, $A_{12}(t) := \frac{\partial f_0}{\partial \eta}(\hat{\varphi}_z^\star(t), 0, \xi, \alpha^\star)$, $A_{13}(t) := \frac{\partial f_0}{\partial \alpha}(\hat{\varphi}_z^\star(t), 0, \xi, \alpha^\star)$, and $A_{22} := F$. The structure of $A(t)$ in (46) then results in the following solution for the VE

$$\Phi_a^\star(t) = \begin{bmatrix} \Phi_{11}^\star(t) & \Phi_{12}^\star(t) & \Phi_{13}^\star(t) & 0 \\ 0 & \Phi_{22}^\star(t) & 0 & 0 \\ 0 & 0 & I & 0 \\ 0 & 0 & 0 & I \end{bmatrix}, \tag{47}$$

where

$$\begin{aligned}
\dot{\Phi}^\star_{11}(t) &= A_{11}(t)\,\Phi^\star_{11}(t), && \Phi^\star_{11}(0) = I\\
\dot{\Phi}^\star_{12}(t) &= A_{11}(t)\,\Phi^\star_{12}(t) + A_{12}(t)\,\Phi^\star_{22}(t), && \Phi^\star_{12}(0) = 0\\
\dot{\Phi}^\star_{13}(t) &= A_{11}(t)\,\Phi^\star_{13}(t) + A_{13}(t), && \Phi^\star_{13}(0) = 0\\
\Phi^\star_{22}(t) &= \exp(F(\varepsilon)\,t).
\end{aligned}$$

We now consider the saltation matrix

$$\Pi_a := I - \frac{f_a\left(x_a^\star\right)\frac{\partial s_a}{\partial x_a}\left(x_a^\star\right)}{\frac{\partial s_a}{\partial x_a}\left(x_a^\star\right) f_a\left(x_a^\star\right)}, \tag{48}$$

in which $x_a^\star := (z^{\star\top}, 0, \alpha^{\star\top}, \xi^\top)^\top$ denotes the augmented fixed point. Using (37), the saltation matrix becomes

$$\Pi_a = \begin{bmatrix} \Pi_{11} & \Pi_{12} & 0 & 0\\ 0 & I & 0 & 0\\ 0 & 0 & I & 0\\ 0 & 0 & 0 & I \end{bmatrix}, \tag{49}$$

where

$$\Pi_{11} := I - \frac{f_0\left(z^\star, 0, \xi, \alpha^\star\right)\frac{\partial \hat{s}}{\partial z}\left(z^\star, 0, \xi\right)}{\frac{\partial \hat{s}}{\partial z}\left(z^\star, 0, \xi\right)\, f_0\left(z^\star, 0, \xi, \alpha^\star\right)} \tag{50}$$

$$\Pi_{12} := -\frac{f_0\left(z^\star, 0, \xi, \alpha^\star\right)\frac{\partial \hat{s}}{\partial \eta}\left(z^\star, 0, \xi\right)}{\frac{\partial \hat{s}}{\partial z}\left(z^\star, 0, \xi\right)\, f_0\left(z^\star, 0, \xi, \alpha^\star\right)}. \tag{51}$$

From (38), (39), (23), and Item 3 of Lemma 2, the Jacobian of the augmented reset map, evaluated at $x_a^\star$, can be expressed as

$$\Upsilon_a := \frac{\partial \Delta_a}{\partial x_a}\left(x_a^\star\right) = \begin{bmatrix} \Upsilon_{11} & \Upsilon_{12} & 0 & 0\\ 0 & \Upsilon_{22} & 0 & 0\\ \Upsilon_{31} & 0 & 0 & 0\\ 0 & 0 & 0 & I \end{bmatrix}, \tag{52}$$

in which $\Upsilon_{11} := \frac{\partial \hat{\Delta}_z}{\partial z}(z^\star, 0, \xi)$, $\Upsilon_{12} := \frac{\partial \hat{\Delta}_z}{\partial \eta}(z^\star, 0, \xi)$, $\Upsilon_{22} := \frac{\partial \hat{\Delta}_\eta}{\partial \eta}(z^\star, 0, \xi)$, and $\Upsilon_{31} := \frac{\partial v}{\partial z}(z^\star, \xi)$. Finally, from [22, Appendix D], the Jacobian of the augmented Poincaré map, evaluated at the fixed point $x_a^\star$, is given by

$$\mathrm{D}P_a\left(x_a^\star\right) = \Pi_a\,\Phi_a^\star\left(T^\star\right)\,\Upsilon_a \tag{53}$$

which in combination with (47), (49), and (52) results in

$$\mathrm{D}_z\hat{P}_z\left(z^\star,0,\alpha^\star,\xi\right)=\Pi_{11}\left\{\Phi^\star_{11}\left(T^\star\right)\Upsilon_{11}+\Phi^\star_{13}\left(T^\star\right)\Upsilon_{31}\right\} \tag{54}$$

$$\mathrm{D}_\eta\hat{P}_z\left(z^\star,0,\alpha^\star,\xi\right)=\Pi_{11}\left\{\Phi^\star_{11}\left(T^\star\right)\Upsilon_{12}+\Phi^\star_{12}\left(T^\star\right)\Upsilon_{22}\right\}+\Pi_{12}\Phi^\star_{22}\left(T^\star\right)\Upsilon_{22} \tag{55}$$

$$\mathrm{D}_\eta\hat{P}_\eta\left(z^\star,0,\alpha^\star,\xi\right)=\Phi^\star_{22}\left(T^\star\right)\Upsilon_{22}=\exp\left(F(\varepsilon)\,T^\star\right)\Upsilon_{22}. \tag{56}$$

This completes the proof of Part (3). □

Remark 3. Equations (54)-(56) together with Part (3) of Theorem 1 present important improvements with respect to [42]. In particular, [42] did *not* consider *parameterized* hybrid zero dynamics (HZD) manifolds. In addition, it did *not* address the effect of the hybrid-invariance event-based controller on the structure of the Jacobian matrix of the Poincaré map. From Part (3) of Theorem 1, the contribution of the event-based controller on the Jacobian matrix can now be seen in two different places. The first one is explicit and includes the $(3,1)$ block of the Jacobian matrix, i.e., $\mathrm{D}_z v(z^*,\xi)$. The second place is implicit and includes the term $\Pi_{11}\Phi^\star_{13}\left(T^\star\right)\Upsilon_{31}$ in (54) (tangent coordinates). Finally, (54) presents a systematic approach to compute the Jacobian of the parameterized restricted map as given in the following corollary.

Corollary 1 (Numerical Approach for Computing the Parameterized Restricted Poincaré Map)**.** Consider the parameterized zero dynamics $\dot{z}=f_0(z,0,\xi,\alpha)$ and let $\Phi^\star_{11}(t,\xi)$ and $\Phi^\star_{13}(t,\xi)$ denote the solution of the following parameterized VEs

$$\dot{\Phi}^\star_{11}(t,\xi)=\frac{\partial f_0}{\partial z}\left(z,0,\xi,\alpha^\star\right)\big|_{z=\hat{\varphi}^\star_z(t)}\ \Phi^\star_{11}(t,\xi),\qquad \Phi^\star_{11}(0,\xi)=I$$

$$\dot{\Phi}^\star_{13}(t,\xi)=\frac{\partial f_0}{\partial z}\left(z,0,\xi,\alpha^\star\right)\big|_{z=\hat{\varphi}^\star_z(t)}\ \Phi^\star_{13}(t,\xi)+\frac{\partial f_0}{\partial \alpha}\left(z,0,\xi,\alpha^\star\right)\big|_{z=\hat{\varphi}^\star_z(t)},\quad \Phi^\star_{13}(0,\xi)=0$$

for $t\in[0,T^\star]$. Then, the Jacobian of the parameterized Poincaré map along

the z-coordinates and restricted to $\hat{\mathcal{S}}_\xi \cap \mathcal{Z}(\xi, \alpha^\star)$ can be computed as follows[5]

$$\mathrm{D}_z \hat{P}_z\left(z^\star, 0, \alpha^\star, \xi\right) = \pi_{\mathrm{proj}}(\xi)\, \Pi_{11}(\xi) \left\{ \underbrace{\Phi^\star_{11}(T^\star, \xi)\, \Upsilon_{11}(\xi)}_{\text{Zero Dynamics Portion}} + \underbrace{\Phi^\star_{13}(T^\star, \xi)\, \Upsilon_{31}(\xi)}_{\text{Event-based Portion}} \right\} \pi_{\mathrm{lift}}(\xi), \tag{57}$$

in which Π_{11}, Υ_{11}, and Υ_{31} were defined in (50) and (52). In (57), we make use of the notation "(ξ)" to highlight the dependence on ξ. Finally, $\pi_{\mathrm{proj}}(\xi) \in \mathbb{R}^{(k-1)\times k}$ and $\pi_{\mathrm{lift}} \in \mathbb{R}^{k\times(k-1)}$ are parameterized projection and lift matrices satisfying the following conditions

$$\pi_{\mathrm{proj}}(\xi)\, \pi_{\mathrm{lift}}(\xi) \qquad = I_{(k-1)\times(k-1)} \tag{58}$$

$$\frac{\partial \hat{s}}{\partial z}\left(z^\star, 0, \xi\right)\, \pi_{\mathrm{lift}}(\xi) = 0. \tag{59}$$

The following theorem makes use of the results of Theorem 1 and Corollary 1 to present the reduced-order stabilization framework.

Theorem 2 (Reduced-Order Stabilization Framework)**.** There exists $\bar{\varepsilon} > 0$ such that for all $0 < \varepsilon < \bar{\varepsilon}$ and $\xi \in \Xi$,

$$\rho\left(\mathrm{D}_z \hat{P}_z\left(z^\star, 0, \alpha^\star, \xi\right)\right) < 1 \tag{60}$$

implies that

1. $\hat{\mathcal{O}}_a = \hat{\mathcal{O}}_z \times \{0\} \times \{\alpha^\star\} \times \{\xi\}$ is stable for the augmented system (40); and
2. $\hat{\mathcal{O}}_z \times \{0\} \times \{\alpha^\star\}$ is exponentially stable for (34).

In our notation, $\rho(.)$ denotes the spectral radius of a matrix.

Proof. See Appendix A. □

Remark 4. Theorem 2 reduces the optimization problem (3) and (4) into the following one

$$\min_{(\xi, W_z, \gamma)} \mathcal{J}\left(\xi, \gamma\right) \tag{61}$$

$$\text{s.t.} \quad \mathcal{I}\left(\mathrm{D}_z \hat{P}_z\left(z^\star, 0, \alpha^\star, \xi\right), W_z, \gamma\right) > 0, \tag{62}$$

[5]In (54), $\mathrm{D}_z \hat{P}_z\left(z^\star, 0, \alpha^\star, \xi\right)$ is considered from $\mathbb{R}^k$ into $\mathbb{R}^k$. However here, we consider it from the $k-1$ dimensional tangent space $\mathsf{T}_{(z^\star,0)}\hat{\mathcal{S}}_\xi \cap \mathcal{Z}(\xi, \alpha^\star)$ back to $\mathsf{T}_{(z^\star,0)}\hat{\mathcal{S}}_\xi \cap \mathcal{Z}(\xi, \alpha^\star)$.

in which $W_z = W_z^\top \in \mathbb{R}^{(k-1)\times(k-1)}$ is a lower-dimensional positive definite Lyapunov matrix. We remark that the optimization problem (61) and (62) requires $p + \frac{k(k-1)}{2} + 1$ decision variables rather than $p + \frac{n(n-1)}{2} + 1$, required for the original one in (3) and (4).

4. Application to Underactuated 3D Bipedal Walking

Virtual constraints are a set of kinematic relations among generalized coordinates enforced asymptotically by continuous-time control inputs [2, 43, 7, 35, 36, 44, 45, 46, 28, 47, 48]. They are defined to coordinate the links of bipedal robots within a stride. In this approach, a set of holonomic output functions $y(x)$ are defined for the continuous-time portion of the hybrid models of bipedal robots and then I-O linearizing controllers [41] are employed to regulate the outputs. Virtual constraint controllers have been numerically and experimentally validated for 2D and 3D underactuated bipedal robots [46, 28, 16, 49, 26] as well as 2D powered prosthetic legs [45, 44, 50, 51]. For mechanical systems with more than one degree of underactuation, the stability of walking gaits depends on the choice of virtual constraints [35, 25]. Our recent approach [35, 37] applied the optimization problem (3) and (4) for the full-order hybrid systems to search for stabilizing virtual constraints. The objective of this section is to employ the reduced-order optimization framework (61) and (62) to systematically look for stabilizing virtual constraints using a smaller set of decision variables.

For the purpose of this paper, we consider a parameterized family of virtual constrains as follows

$$y(q, \xi, \alpha) := H(\xi)\,(q - q_{\mathrm{d}}(\theta)) - h_{\mathrm{corr}}(\theta, \alpha), \tag{63}$$

where q and $q_{\mathrm{d}}(\theta)$ denote the generalized coordinates of the mechanical system and their desired evolution on the periodic gait in terms of the phasing variable θ, respectively. We remark that the virtual constraints in (63) have the structure of the parameterized output functions presented in Example 1 for which the uniform relative degree is 2 (i.e., $r = 2$) due to the second-order nature of the Lagrangian continuous-time models. $H(\xi)\,q$ represents a set of holonomic variables to be controlled, referred to as the *controlled variables*. The objective is to search for the output matrix $H(\xi)$, or equivalently the controlled variables, to guarantee the exponential stability of periodic walking gaits. The corrective term here is defined in a piece-wise manner as given in (14) for which $b(\theta, \alpha)$ is taken as a Bézier polynomial analogous to [25].

4.1. ATRIAS: An Underactuated 3D Bipedal Robot

ATRIAS is an underactuated bipedal robot designed for robust and energy efficient 3D walking. The robot's structure includes a torso with two identical legs terminating in point feet (see Fig. 3). More details about the robot's model can be found in [26, 52]. Two motors in series with harmonic drives are used to drive each leg in the sagittal plane. In the frontal plane, each of the hip joints is driven by a motor located in the torso. In total, the robot has 6 brushless DC motors.

The orientation of the torso frame with respect to an inertial world frame can be described by thee Euler angles $q_{z\mathrm{T}}$ (yaw), $q_{y\mathrm{T}}$ (roll), and $q_{x\mathrm{T}}$ (pitch) (see Fig. 3). In the sagittal plane, the angles of the shin and thigh links with respect to the torso are denoted by $q_{1\mathrm{R}}$ and $q_{2\mathrm{R}}$ for the right leg and $q_{1\mathrm{L}}$ and $q_{2\mathrm{L}}$ for the left leg. The angles of the corresponding harmonic drives with respect to the torso are then represented by q_{gr1R}, q_{gr2R}, q_{gr1L}, and q_{gr2L} (see again Fig. 3). The torques generated by the sagittal plane DC motors are also denoted by $u_{1\mathrm{R}}$, $u_{2\mathrm{R}}$, $u_{1\mathrm{L}}$, and $u_{2\mathrm{L}}$. In the frontal plane, the angles of the right and left hips with respect to the torso are represented by $q_{3\mathrm{R}}$ and $q_{3\mathrm{L}}$, respectively. Finally, $u_{3\mathrm{R}}$ and $u_{3\mathrm{L}}$ denote the corresponding torques generated by the frontal plane DC motors.

During the single support phase, the robot has 13 DOFs. In particular, the generalized coordinates vector can be expressed as

$$q := \left(q_{\mathrm{u}}^{\top}, q_{\mathrm{a}}^{\top}\right)^{\top} \in \mathbb{R}^{13}, \tag{64}$$

where q_{u} and q_{a} denote the unactuated and actuated DOFs, respectively, defined as follows

$$q_{\mathrm{u}} := \left(q_{z\mathrm{T}}, q_{y\mathrm{T}}, q_{x\mathrm{T}}, q_{1\mathrm{R}}, q_{2\mathrm{R}}, q_{1\mathrm{L}}, q_{2\mathrm{L}}\right)^{\top} \in \mathbb{R}^{7} \tag{65}$$

$$q_{\mathrm{a}} := \left(q_{\mathrm{gr1R}}, q_{\mathrm{gr2R}}, q_{3\mathrm{R}}, q_{\mathrm{gr1L}}, q_{\mathrm{gr2L}}, q_{3\mathrm{L}}\right)^{\top} \in \mathbb{R}^{6}. \tag{66}$$

The control input vector can also be given by

$$u := \left(u_{1\mathrm{R}}, u_{2\mathrm{R}}, u_{3\mathrm{R}}, u_{1\mathrm{L}}, u_{2\mathrm{L}}, u_{3\mathrm{L}}\right)^{\top} \in \mathbb{R}^{6}. \tag{67}$$

Based on the left-right symmetry, one can present an open-loop hybrid model with one continuous-time phase, as given in (6), to describe the 3D walking motion of ATRIAS [35, Theorem 4]. In particular, the evolution of the

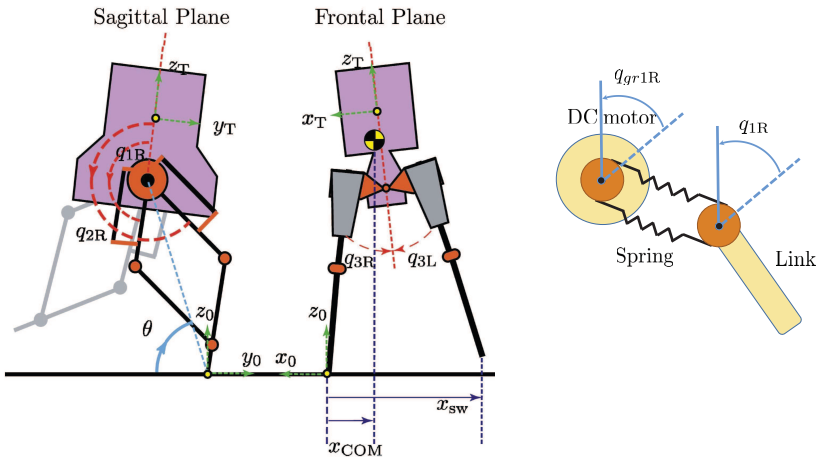

Figure 3: Sagittal and frontal planes of ATRIAS during the right stance phase with the associated configuration variables [35]. The Euler angles describe the orientation of the tors frame $O_T x_T y_T z_T$ with respect to the world frame $O_0 x_0 y_0 z_0$. The right figure is a conceptual representation of series elastic actuators employed in the sagittal plane of ATRIAS.

system during the continuous-time phase can be represented by the following dynamics arising from the Euler-Lagrange equation

$$D_{\mathrm{uu}}(q)\,\ddot{q}_{\mathrm{u}} + D_{\mathrm{ua}}(q)\,\ddot{q}_{\mathrm{a}} + N_{\mathrm{u}}(q,\dot{q}) = 0 \tag{68}$$

$$D_{\mathrm{au}}(q)\,\ddot{q}_{\mathrm{u}} + D_{\mathrm{aa}}(q)\,\ddot{q}_{\mathrm{a}} + N_{\mathrm{a}}(q,\dot{q}) = B_{\mathrm{a}}\,u \tag{69}$$

where $D_{\mathrm{uu}} \in \mathbb{R}^{7\times 7}$, $D_{\mathrm{ua}} \in \mathbb{R}^{7\times 6}$, $D_{\mathrm{au}} \in \mathbb{R}^{6\times 7}$, and $D_{\mathrm{aa}} \in \mathbb{R}^{6\times 6}$ denote the sub-matrices of the positive-definite mass-inertia matrix. $N_{\mathrm{u}} \in \mathbb{R}^7$ and $N_{\mathrm{a}} \in \mathbb{R}^6$ represent the unactuated and actuated decomposition of the Coriolis, centrifugal, gravity, and spring-damper terms. Furthermore, $B_{\mathrm{a}} \in \mathbb{R}^{6\times 6}$ is the input distribution matrix with the property $\mathrm{rank} B_{\mathrm{a}} = 6$. The reset map Δ in (6) is also constructed based on the rigid and instantaneous impact model of the swing leg end with the ground [1]. The switching manifold $\mathcal{S}$ is finally chosen as the set of all state vectors $x := (q^\top, \dot{q}^\top)^\top$ for which the swing leg end contacts the flat ground.

4.2. Parameterized Zero Dynamics for ATRIAS

Using the motion planning algorithm of [26], a periodic gait is designed for walking at the speed of 1.1 (m/s) to satisfy Assumption 1. The phasing

variable θ is then defined as the angle of the virtual line connecting the stance leg end to the hip joint in the sagittal plane to fulfill Assumption 2 (see Fig. 3). For the ATRIAS structure, θ is only a function of unactuated coordinates and can be given by $\theta = \theta(q_{\mathrm{u}})$. The virtual constraints in (63) can then be decomposed as follows

$$\begin{aligned} y(q,\xi,\alpha) &= \begin{bmatrix} H_{\mathrm{u}}(\xi) & H_{\mathrm{a}}(\xi) \end{bmatrix} \begin{bmatrix} q_{\mathrm{u}} - q_{\mathrm{ud}}(\theta) \\ q_{\mathrm{a}} - q_{\mathrm{ad}}(\theta) \end{bmatrix} - h_{\mathrm{corr}}(\theta,\alpha) \\ &= 0, \end{aligned} \tag{70}$$

where $H_{\mathrm{u}}(\xi) \in \mathbb{R}^{6\times 7}$ and $H_{\mathrm{a}}(\xi) \in \mathbb{R}^{6\times 6}$ are the corresponding sub-matrices of $H(\xi)$ with the assumption $\mathrm{rank} H_{\mathrm{a}}(\xi) = 6$ for every $\xi \in \Xi$. In addition, $q_{\mathrm{ud}}(\theta)$ and $q_{\mathrm{ad}}(\theta)$ denote the desired evolutions of the unactuated and actuated coordinates on the orbit $\mathcal{O}$ in terms of θ, respectively. From (70), one can obtain the evolution of the actuated coordinates on the parameterized zero dynamics manifold $\mathcal{Z}(\xi,\alpha)$ in terms of (q_u,ξ,α) as follows

$$\begin{aligned} q_{\mathrm{a}} &= q_{\mathrm{ad}}(\theta) - H_{\mathrm{a}}^{-1}(\xi)\, H_{\mathrm{u}}(\xi)\, (q_{\mathrm{u}} - q_{\mathrm{ud}}(\theta)) + H_{\mathrm{a}}^{-1}(\xi)\, h_{\mathrm{corr}}(\theta,\alpha) \\ &=: \hat{q}_{\mathrm{ad}}(q_u,\xi,\alpha) \end{aligned} \tag{71}$$

which results in the position lift map

$$q = \begin{bmatrix} q_{\mathrm{u}} \\ \hat{q}_{\mathrm{ad}}(q_u,\xi,\alpha) \end{bmatrix} =: \hat{q}_{\mathrm{d}}(q_u,\xi,\alpha). \tag{72}$$

Substituting (71) and (72) in (68) then results in the following 14-dimensional parameterized zero dynamics

$$D_{\mathrm{zero}}(q_{\mathrm{u}},\xi,\alpha)\, \ddot{q}_{\mathrm{u}} + N_{\mathrm{zero}}(q_{\mathrm{u}},\dot{q}_{\mathrm{u}},\xi,\alpha) = 0, \tag{73}$$

where

$$\begin{aligned} D_{\mathrm{zero}}(q_{\mathrm{u}},\xi,\alpha) \quad &:= D_{\mathrm{uu}}\left(\hat{q}_{\mathrm{d}}(q_{\mathrm{u}},\xi,\alpha)\right) \\ &\quad + D_{\mathrm{ua}}\left(\hat{q}_{\mathrm{d}}(q_{\mathrm{u}},\xi,\alpha)\right) \frac{\partial \hat{q}_{\mathrm{ad}}}{\partial q_u}\,(q_u,\xi,\alpha) \\ N_{\mathrm{zero}}(q_{\mathrm{u}},\dot{q}_{\mathrm{u}},\xi,\alpha) &:= N_{\mathrm{u}}\left(\hat{q}_{\mathrm{d}}(q_{\mathrm{u}},\xi,\alpha), \dot{\hat{q}}_{\mathrm{d}}(q_{\mathrm{u}},\dot{q}_{\mathrm{u}},\xi,\alpha)\right) \\ &\quad + D_{\mathrm{ua}}\left(\hat{q}_{\mathrm{d}}(q_{\mathrm{u}},\xi,\alpha)\right) \frac{\partial}{\partial q_{\mathrm{u}}} \left(\frac{\partial \hat{q}_{\mathrm{ad}}}{\partial q_{\mathrm{u}}}(q_{\mathrm{u}},\xi,\alpha)\, \dot{q}_{\mathrm{u}}\right) \dot{q}_{\mathrm{u}}. \end{aligned}$$

Based on (73), the tangent coordinates can be chosen as $z(x) := (q_{\mathrm{u}}^\top, \dot{q}_{\mathrm{u}}^\top)^\top \in \mathbb{R}^{14}$ to satisfy Assumption 4. Finally for the ATRIAS structure, we remark that the full and restricted Poincaré maps are 25- and 13-dimensional, respectively.

4.3. Numerical Results

For bipedal robots with yaw motion, there are two kinds of stability during waling: *full-state stability* and *stability-modulo yaw*. The stability modulo yaw refers to the stability in $\mathcal{X} \setminus \mathbb{S}^1$, where $\mathbb{S}^1 := [0, 2\pi)$ denotes the unit circle [5, 53] and "\" represents the set difference. We will apply the reduced-order framework for the stability modulo yaw and full-state stability in Sections 4.3.1 and 4.3.2, respectively. To solve the optimization problem (61) and (62), we employ the bilinear matrix inequality (BMI) algorithm developed in [35]. The algorithm is based on the sensitivity analysis and BMIs for which the cost function is chosen as

$$\mathcal{J}(\xi, \gamma) = -w\gamma + \frac{1}{2} \left\| \xi - \xi^\star \right\|_2^2, \tag{74}$$

where $\xi^\star$ represents a nominal set of continuous-time parameters and $w > 0$ is a weighting factor. In addition, the algorithm approximates the nonlinear matrix inequality (62) by a BMI based on its Taylor series expansion around $\xi^\star$. The cost function (74) tries to improve the convergence rate while keeping the continuous-time parameters close enough to the nominal ones to have a good approximation for the Taylor series. To numerically solve the BMI algorithm of [35], we then employ the PENBMI solver from TOMLAB [54, 55] integrated with the MATLAB environment through the YALMIP [56]. For the purpose of this paper, the nominal parameters $\xi^\star$, or equivalently the nominal controlled variables, are chosen as

$$H^\star q = \begin{bmatrix} \frac{1}{2}\left(q_{\mathrm{gr1R}} + q_{\mathrm{gr2R}}\right) \\ \frac{1}{2}\left(q_{\mathrm{gr1L}} + q_{\mathrm{gr2L}}\right) \\ q_{\mathrm{gr2R}} - q_{\mathrm{gr1R}} \\ q_{\mathrm{gr2L}} - q_{\mathrm{gr1L}} \\ q_{\mathrm{3R}} \\ -q_{y\mathrm{T}} + q_{\mathrm{3L}} \end{bmatrix}. \tag{75}$$

The first two components of the controlled variables in (75) represent the leg angles for the right and left legs. The leg angle is defined as the angle between the torso and the virtual line connecting the hip joint to the leg end. We remark that for the ATRIAS structure, the legs are actuated through springs and hence, the leg angles are defined at the outputs of the harmonic drives. The third and fourth components of the controlled variables in (75) are then taken as the right and left knee angles, respectively. The fifth and sixth

components are finally defined in the frontal plane. In particular, the fifth component represents the stance hip angle, whereas the sixth component is defined as the absolute swing hip angle.

4.3.1. Stability Modulo Yaw

Corresponding to the nominal controlled variables given in (75), the dominant eigenvalues of the 13-dimensional restricted Poincaré map become $\{-1.3060, -1.000, 0.8815, -0.1221\}$ and consequently, the gait is not stable. From [35], the eigenvalue -1 corresponds to the yaw coordinates. We have observed that the first four components of the controlled variables in (75) can stabilize walking gaits for the planar (i.e., 2D) model of ATRIAS [26]. To improve the stability of the gait, one can then focus on the lateral stability. For this purpose, we let $\xi = (\xi_1, \cdots, \xi_6)^\top \in \mathbb{R}^6$ only parameterize the second column of the output matrix H that corresponds to the torso roll angle $q_{y\mathrm{T}}$. In particular, we parameterize the output matrix as follows

$$H(\xi) = H^\star + \sum_{i=1}^{6} E_{i,2}\, \xi_i, \tag{76}$$

where for every $i \in \{1, 2, \cdots, 6\}$, $E_{i,2} \in \mathbb{R}^{6\times 13}$ is a matrix whose elements are zero except the $(i, 2)$ component. The reduced-order optimization framework (61) and (62) then requires $6 + \frac{14\times 13}{2} + 1 = 98$ decision variables, whereas the original one in (3) and (4) requires $6 + \frac{26\times 25}{2} + 1 = 332$ variables (i.e. 70% decrease in the number of decision variables). A local optimal solution for the BMI algorithm is numerically computed as follows

$$H(\xi)\, q = \begin{bmatrix} \frac{1}{2}\left(q_{\mathrm{gr1R}} + q_{\mathrm{gr2R}}\right) \\ \frac{1}{2}\left(q_{\mathrm{gr1L}} + q_{\mathrm{gr2L}}\right) \\ q_{\mathrm{gr2R}} - q_{\mathrm{gr1R}} \\ q_{\mathrm{gr2L}} - q_{\mathrm{gr1L}} \\ q_{3\mathrm{R}} \\ -q_{y\mathrm{T}} + q_{3\mathrm{L}} \end{bmatrix} + \underbrace{\begin{bmatrix} -0.5574 \\ 0.4878 \\ -0.0162 \\ 0.0735 \\ -0.2613 \\ -0.3884 \end{bmatrix}}_{\xi} q_{y\mathrm{T}} \tag{77}$$

for which the dominant eigenvalues of the restricted Poincaré map become $\{-1.0000, 0.7067, -0.1577 \pm 0.5296i\}$. Hence, the optimal controlled variables in (77) exponentially stabilize the gait modulo yaw. Figure 4 depicts the phase portraits of the closed-loop hybrid system during 100 consecutive steps.

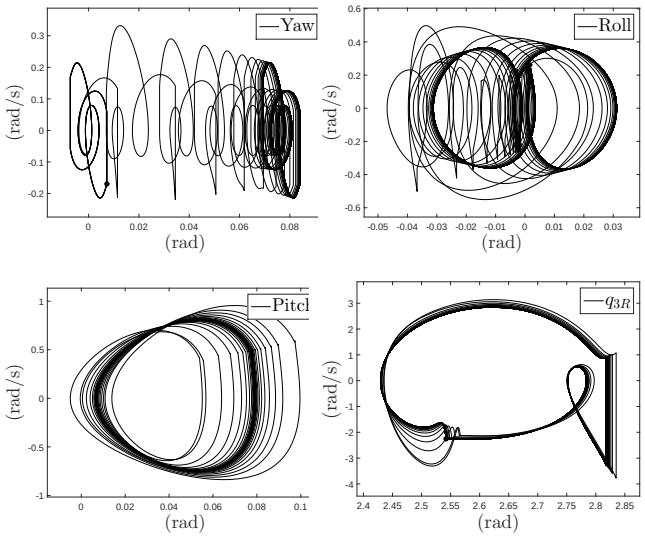

Figure 4: Phase portraits of the closed-loop hybrid system for the Euler angles and right hip during 100 consecutive steps corresponding to the optimal solutions of (61) and (62) for stability modulo yaw. The circles represent the initial condition of the simulator.

Here, the simulation starts at the beginning of the right stance phase on the orbit. During the tenth step, an external horizontal force with a magnitude of 100 (N) is applied to the COM of the robot in the frontal plane for 40% of the step. Convergence to the periodic orbit in all coordinates except the yaw motion is clear. We remark that the periodic gait $\mathcal{O}$ has been designed to walk along the y-axis of the world frame which corresponds to the yaw angle $q_{z\mathrm{T}}$ being zero. However, since the orbit is exponentially stable modulo yaw, the external force changes the direction of walking by shifting the phase portrait in the yaw coordinates. The animation of this simulation can be found at [57].

4.3.2. Full-State Stability

Starting with the optimized controlled variables in (77) as the nominal parameters, we now consider the full-state stabilization problem. For this purpose, we let ξ parameterize the first column of the H matrix that corresponds to the yaw motion. In particular,

$$H(\xi) = H_{\mathrm{opt}} + \sum_{i=1}^{6} E_{i,1}\, \xi_i, \tag{78}$$

where H_{opt} represents the output matrix obtained in (77) for stability modulo yaw. Furthermore for every $i \in \{1, 2, \cdots, 6\}$, $E_{i,1} \in \mathbb{R}^{6\times 13}$ is a matrix whose elements are zero except the $(i, 1)$ component. For this set of output matrices, the optimal controlled variables become

$$H(\xi)\, q = \begin{bmatrix} \frac{1}{2}\left(q_{\text{gr1R}} + q_{\text{gr2R}}\right) \\ \frac{1}{2}\left(q_{\text{gr1L}} + q_{\text{gr2L}}\right) \\ q_{\text{gr2R}} - q_{\text{gr1R}} \\ q_{\text{gr2L}} - q_{\text{gr1L}} \\ q_{\text{3R}} \\ -q_{y\text{T}} + q_{\text{3L}} \end{bmatrix} + \begin{bmatrix} -0.5574 \\ 0.4878 \\ -0.0162 \\ 0.0735 \\ -0.2613 \\ -0.3884 \end{bmatrix} q_{y\text{T}} + \underbrace{\begin{bmatrix} 0.2697 \\ -0.1641 \\ -0.0266 \\ -0.0130 \\ -0.1375 \\ -0.0266 \end{bmatrix}}_{\xi} q_{z\text{T}} \tag{79}$$

for which the dominant eigenvalues of the restricted Poincaré map are {0.7449,-0.7154,-0.4938±0.3453i}. To confirm the numerical results, Fig. 5 represents the phase portraits of the closed-loop system during 100 consecutive steps. Here the simulation starts at the initial condition of Fig. 4. During the tenth step, an external horizontal force with a magnitude of 100 (N) is applied to the COM of the robot in the frontal plane for 40% of the step. The convergence to the periodic orbit even in the yaw coordinates is clear. The animation of this simulation can be found at [57].

5. Conclusion

Hybrid systems have become a very common language for representing the dynamics of bipedal robots and for posing feedback control design problems. For obvious reasons, equilibrium points are of less interest than periodic orbits in such robots and thus this paper focuses on the stabilization of periodic orbits through offline optimization. The quest for greater mobility is driving an increase in the mechanical complexity of these robots, which manifests itself in higher-dimensional dynamical models, and thus in optimization problems with ever more variables. The key contribution of the paper was to show how controlled-invariant manifolds in the hybrid setting can be used to pare down the size of the optimization problem.

This paper introduced a reduced-order framework to exponentially stabilize periodic orbits on a parameterized family of hybrid invariant manifolds. Our previous work developed an optimization framework to systematically choose stabilizing controllers from a family of parameterized feedback laws.

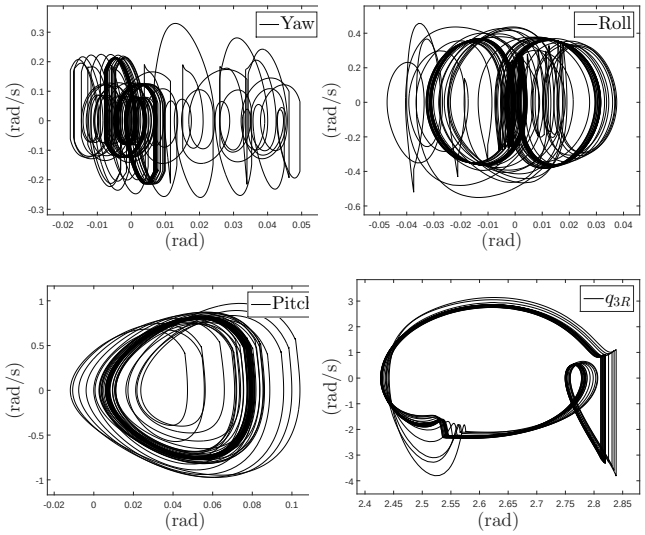

Figure 5: Phase portraits of the closed-loop hybrid system for the Euler angles and right hip during 100 consecutive steps corresponding to the optimal solutions of (61) and (62) for full-state stability. The circles represent the initial condition of the simulator.

The optimization problem looks for controller parameters as well as a set of Lyapuonv matrices to stabilize the orbits. One drawback of applying the optimization problem for the full-order models is that for bipedal robots with high DOFs, the number of entries in the Lyapunov matrices becomes dominant that makes the stabilization problem prohibitive. To address this challenge, the current paper assumed a family of parameterized output functions to be regulated for the continuous-time portion of the hybrid system using I-O linearizing controllers. In addition, it considered a family of parameterized event-based update laws to make the corresponding zero dynamics manifolds hybrid invariant. We then investigated the properties of the parameterized Poincaré map to translate the full-order optimization problem into a reduced-order one on the family of parameterized HZD manifolds.

The key features of the reduced-order framework are as follows: (1) it accounts for underactuation; (2) it significantly reduces the number of decision variables for the optimization-based stabilization problem; (3) it investigates the effect of output parameters and event-based update laws on the Poincaré map; and (4) finally the framework presents a systematic approach to compute the Jacobian linearization of the parameterized Poincaré. To illustrate the power of the algorithm, the paper then employed the reduced-

order framework to systematically design stabilizing I-O linearizing controller for walking gaits of a 3D bipedal robot with 13 DOFs and 7 degrees of underactuation.

Appendix A. Proof of Theorem 2

By defining $x_1 := (z^\top, \eta^\top, \alpha^\top)^\top$ and $x_2 := \xi$, the augmented hybrid system (40) can be rewritten in the following compact form

$$\hat{\Sigma}_a^{\mathrm{cl}} : \begin{cases} \begin{bmatrix} \dot{x}_1 \\ \dot{x}_2 \end{bmatrix} = \begin{bmatrix} f_1(x_1, x_2) \\ 0 \end{bmatrix}, & \begin{bmatrix} x_1^- \\ x_2^- \end{bmatrix} \notin \hat{\mathcal{S}}_a \\ \begin{bmatrix} x_1^+ \\ x_2^+ \end{bmatrix} = \begin{bmatrix} \Delta_1\left(x_1^-, x_2^-\right) \\ x_2^- \end{bmatrix}, & \begin{bmatrix} x_1^- \\ x_2^- \end{bmatrix} \in \hat{\mathcal{S}}_a, \end{cases} \tag{A.1}$$

where $f_1 := (f_0^\top, \eta^\top F^\top, 0)^\top$ and $\Delta_1 := (\hat{\Delta}_z^\top, \hat{\Delta}_\eta^\top, v^\top)^\top$. Furthermore for every x_2, $\mathcal{O}_1 \times \{x_2\}$ is a period-one orbit of (A.1), in which $\mathcal{O}_1 := \hat{\mathcal{O}}_z \times \{0\} \times \{\alpha^\star\}$. Using this new notation, the Jacobian of the Poincaré map in (43) can be written as

$$\left[\begin{array}{c|c} A_{11} & 0 \\ \hline 0 & I \end{array}\right],$$

where

$$A_{11} := \begin{bmatrix} \mathrm{D}_z \hat{P}_z(z^\star, 0, \alpha^\star, \xi) & \mathrm{D}_\eta \hat{P}_z(z^\star, 0, \alpha^\star, \xi) & 0 \\ 0 & \mathrm{D}_\eta \hat{P}_\eta(z^\star, 0, \alpha^\star, \xi) & 0 \\ \mathrm{D}_z v(z^\star, \xi) & 0 & 0 \end{bmatrix}.$$

Analogous to the analysis of [42], $\lim_{\varepsilon \searrow 0} \mathrm{D}_\eta \hat{P}_\eta(z^\star, 0, \alpha^\star, \xi) = \lim_{\varepsilon \searrow 0} \exp(F(\varepsilon)T^\star)\Upsilon_{22} = 0$, and hence from continuity of A_{11} with respect to ε, there is $\bar{\varepsilon} > 0$ such that the dominant eigenvalues of A_{11} are determined by those of $\mathrm{D}_z \hat{P}_z(z^\star, \xi, \alpha^\star, 0)$ for all $0 < \varepsilon < \bar{\varepsilon}$. This fact in combination with (60) implies that A_{11} is Schur stable, i.e., all eigenvalues of A_{11} lie inside the unit circle. Next, the decentralized structure of the augmented Poincaré return map on $\hat{\mathcal{S}}_a$ as

$$\begin{bmatrix} x_1[k+1] \\ x_2[k+1] \end{bmatrix} = \begin{bmatrix} P_1(x_1[k], x_2[k]) \\ x_2[k] \end{bmatrix}$$

guarantees the stability of the fixed point $(x_1^{\star\top}, x_2^\top)^\top$ for the fixed $x_2 = \xi$, where $P_1 := (\hat{P}_z^\top, \hat{P}_\eta^\top, v^\top)^\top$ and $x_1^\star := (z^{\star\top}, 0, \alpha^{\star\top})^\top$. In addition, $x_1^\star$ is exponentially stable for $x_1[k+1] = P_1(x_1[k], x_2)$. Now, let us take a point $(x_{10}^\top, x_{20}^\top)^\top \in \hat{\mathcal{S}}_a$ and denote the solution of the hybrid system, starting from

the initial condition $(\Delta_1^\top(x_{10}, x_{20}), x_{20}^\top)^\top$, by $(\varphi_1^\top(t), \varphi_2^\top(t))^\top$. Suppose further that t_1 represents the first time at which the solution intersects $\hat{\mathcal{S}}_a$. Then applying inequality (C.6) of [58] implies that

$$\begin{aligned}\sup_{0\le t\le t_1} \operatorname{dist}\left(\begin{bmatrix}\varphi_1(t)\\ \varphi_2(t)\end{bmatrix}, \mathcal{O}_1 \times \{x_2\}\right) &\le L \left\|\begin{bmatrix}x_{10} - x_1^\star\\ x_{20} - x_2\end{bmatrix}\right\| \\ &\le L\,\|x_{10} - x_1^\star\| + L\,\|x_{20} - x_2\| \qquad \text{(A.2)}\end{aligned}$$

for some $L > 0$. Finally, one can apply the ϵ-δ requirements to show that $x_1^\star$ being exponentially stable for $x_1[k+1] = P_1(x_1[k], x_2)$ implies $\mathcal{O}_1 \times \{x_2\}$ is stable for (A.1). In particular for every $\epsilon > 0$, there is $\delta > 0$ such that

$$\left\|\begin{bmatrix}x_{10} - x_1^\star\\ x_{20} - x_2\end{bmatrix}\right\| < \delta$$

results in

$$\operatorname{dist}\left(\begin{bmatrix}\varphi_1(t)\\ \varphi_2(t)\end{bmatrix}, \mathcal{O}_1 \times \{x_2\}\right) < \epsilon.$$

This completes the proof of Part (1). For Part (2) when x_{20} is set to x_2, $\varphi_2(t) \equiv x_2$ and hence, the inequality (A.2) reduces to

$$\sup_{0\le t\le t_1} \operatorname{dist}\left(\varphi_1(t), \mathcal{O}_1\right) \le L\,\|x_{10} - x_1^\star\|$$

which in turn guarantees the exponential stability of $\mathcal{O}_1$ for (34).

Acknowledgments

The work of K. Akbari Hamed was partially supported by the Center for Sensorimotor Neural Engineering (CSNE) that is an NSF Engineering Research Center. The work of J. W. Grizzle was supported by NSF Grants ECCS-1343720 and NRI-1525006.

References

[1] Y. Hurmuzlu, D. B. Marghitu, Rigid body collisions of planar kinematic chains with multiple contact points, The International Journal of Robotics Research 13 (1) (1994) 82–92. doi:10.1177/027836499401300106.

[2] J. Grizzle, G. Abba, F. Plestan, Asymptotically stable walking for biped robots: analysis via systems with impulse effects, Automatic Control, IEEE Transactions on 46 (1) (2001) 51–64. doi:10.1109/9.898695.

[3] G. Song, M. Zefran, Underactuated dynamic three-dimensional bipedal walking, in: Robotics and Automation. Proceedings IEEE International Conference on, 2006, pp. 854–859. doi:10.1109/ROBOT.2006.1641816.

[4] J. W. Grizzle, C. Chevallereau, R. W. Sinnet, A. D. Ames, Models, feedback control, and open problems of 3D bipedal robotic walking, Automatica 50 (8) (2014) 1955–1988.

[5] M. Spong, F. Bullo, Controlled symmetries and passive walking, Automatic Control, IEEE Transactions on 50 (7) (2005) 1025–1031. doi:10.1109/TAC.2005.851449.

[6] M. Spong, J. Holm, D. Lee, Passivity-based control of bipedal locomotion, Robotics Automation Magazine, IEEE 14 (2) (2007) 30–40. doi:10.1109/MRA.2007.380638.

[7] A. Ames, Human-inspired control of bipedal walking robots, Automatic Control, IEEE Transactions on 59 (5) (2014) 1115–1130. doi:10.1109/TAC.2014.2299342.

[8] A. Ames, K. Galloway, K. Sreenath, J. Grizzle, Rapidly exponentially stabilizing control Lyapunov functions and hybrid zero dynamics, Automatic Control, IEEE Transactions on 59 (4) (2014) 876–891. doi:10.1109/TAC.2014.2299335.

[9] R. Gregg, L. Righetti, Controlled reduction with unactuated cyclic variables: Application to 3D bipedal walking with passive yaw rotation, Automatic Control, IEEE Transactions on 58 (10) (2013) 2679–2685. doi:10.1109/TAC.2013.2256011.

[10] R. Gregg, A. Tilton, S. Candido, T. Bretl, M. Spong, Control and planning of 3-D dynamic walking with asymptotically stable gait primitives, Robotics, IEEE Transactions on 28 (6) (2012) 1415–1423. doi:10.1109/TRO.2012.2210484.

[11] K. Byl, R. Tedrake, Approximate optimal control of the compass gait on rough terrain, in: Robotics and Automation. IEEE International Conference on, 2008, pp. 1258–1263. doi:10.1109/ROBOT.2008.4543376.

[12] C. Saglam, K. Byl, Switching policies for metastable walking, in: Decision and Control, IEEE 52nd Annual Conference on, 2013, pp. 977–983. doi:10.1109/CDC.2013.6760009.

[13] H. Dai, R. Tedrake, $\mathcal{L}_2$-gain optimization for robust bipedal walking on unknown terrain, in: Robotics and Automation, IEEE International Conference on, 2013, pp. 3116–3123. doi:10.1109/ICRA.2013.6631010.

[14] I. R. Manchester, U. Mettin, F. Iida, R. Tedrake, Stable dynamic walking over uneven terrain, The International Journal of Robotics Research 30 (3) (2011) 265–279. doi:10.1177/0278364910395339.

[15] A. Shiriaev, L. Freidovich, S. Gusev, Transverse linearization for controlled mechanical systems with several passive degrees of freedom, Automatic Control, IEEE Transactions on 55 (4) (2010) 893–906. doi:10.1109/TAC.2010.2042000.

[16] A. E. Martin, D. C. Post, J. P. Schmiedeler, The effects of foot geometric properties on the gait of planar bipeds walking under HZD-based control, The International Journal of Robotics Research 33 (12) (2014) 1530–1543. doi:10.1177/0278364914532391.

[17] C. D. Remy, Optimal exploitation of natural dynamics in legged locomotion, Ph.D. thesis, ETH Zurich (2011).

[18] W. Haddad, V. Chellaboina, S. Nersesov, Impulsive and Hybrid Dynamical Systems: Stability, Dissipativity, and Control, Princeton University Press, 2006.

[19] R. Goebel, R. Sanfelice, A. Teel, Hybrid Dynamical Systems: Modeling, Stability, and Robustness, Princeton University Press, 2012.

[20] D. Bainov, P. Simeonov, Systems With Impulse Effect: Stability, Theory and Applications, Ellis Horwood Ltd, 1989.

[21] H. Ye, A. Michel, L. Hou, Stability theory for hybrid dynamical systems, Automatic Control, IEEE Transactions on 43 (4) (1998) 461–474. doi:10.1109/9.664149.

[22] T. Parker, L. Chua, Practical Numerical Algorithms for Chaotic Systems, Springer, 1989.

[23] S. Burden, S. Revzen, S. Sastry, Model reduction near periodic orbits of hybrid dynamical systems, Automatic Control, IEEE Transactions on to appear. doi:10.1109/TAC.2015.2411971.

[24] J. W. Grizzle, Remarks on event-based stabilization of periodic orbits in systems with impulse effects, in: Second International Symposium on Communication, Control and Signal Processing, 2006.

[25] C. Chevallereau, J. Grizzle, C.-L. Shih, Asymptotically Stable Walking of a Five-Link Underactuated 3-D Bipedal Robot, Robotics, IEEE Transactions on 25 (1) (2009) 37–50. doi:10.1109/TRO.2008.2010366.

[26] A. Ramezani, J. Hurst, K. Akbai Hamed, J. Grizzle, Performance analysis and feedback control of ATRIAS, a three-dimensional bipedal robot, Journal of Dynamic Systems, Measurement, and Control December, ASME 136 (2). doi:10.1115/1.4025693.

[27] K. Akbari Hamed, J. Grizzle, Event-based stabilization of periodic orbits for underactuated 3-D bipedal robots with left-right symmetry, Robotics, IEEE Transactions on 30 (2) (2014) 365–381. doi:10.1109/TRO.2013.2287831.

[28] K. Sreenath, H.-W. Park, I. Poulakakis, J. Grizzle, Embedding active force control within the compliant hybrid zero dynamics to achieve stable, fast running on mabel, The International Journal of Robotics Research 32 (3) (2013) 324–345. doi:10.1177/0278364912473344.

[29] M. H. Raibert, Legged robots, Communications of the ACM 29 (6) (1986) 499514.

[30] M. Buehler, D. E. Koditschek, P. J. Kindlmann, Planning and control of robotic juggling and catching tasks, The International Journal of Robotics Research 13 (12) (1994) 101–118. doi:10.1177/027836499401300201.

[31] S. G. Carver, N. J. Cowan, J. M. Guckenheimer, Lateral stability of the spring-mass hopper suggests a two-step control strategy for running, Chaos 19 (2) (2009) 026106. doi:10.1063/1.3127577.

[32] M. M. Ankarali, U. Saranli, Control of underactuated planar pronking through an embedded spring-mass hopper template, Autonomous Robots 30 (2) (2011) 217–231.

[33] J. Seipel, P. Holmes, A simple model for clock-actuated legged locomotion, Regular and Chaotic Dynamics 12 (5) (2007) 502–520.

[34] A. Seyfarth, H. Geyer, H. Herr, Swing-leg retraction: a simple control model for stable running, The Journal of Experimental Biology 206 (15) (2003) 2547–2555. doi:10.1242/jeb.00463.

[35] K. Akbari Hamed, B. Buss, J. Grizzle, Exponentially stabilizing continuous-time controllers for periodic orbits of hybrid systems: Application to bipedal locomotion with ground height variations, The International Journal of Robotics Research (2015) published online-doi:10.1177/0278364915593400.

[36] K. Akbari Hamed, B. Buss, J. Grizzle, Continuous-time controllers for stabilizing periodic orbits of hybrid systems: Application to an underactuated 3D bipedal robot, in: Decision and Control (CDC), 2014 IEEE 53rd Annual Conference on, 2014, pp. 1507–1513. doi:10.1109/CDC.2014.7039613.

[37] K. Akbari Hamed, J. Grizzle, Iterative robust stabilization algorithm for periodic orbits of hybrid dynamical systems: Application to bipedal running, in: The IFAC Conference on Analysis and Design of Hybrid Systems, 2015, accepted to appear.

[38] B. G. Buss, K. Akbari Hamed, B. A. Griffin, J. W. Grizzle, Experimental results for 3D bipedal robot walking based on systematic optimization of virtual constraints, in: The 2016 American Control Conference, 2016, accepted to appear.

[39] Dynamic Leg Locomotion YouTube Channel, MARLO: Dynamic 3D walking based on HZD gait design and BMI constraint selection (2015). URL `https://www.youtube.com/watch?v=5ms5DtPNwHo`

[40] M. Diehl, K. Mombaur, D. Noll, Stability optimization of hybrid periodic systems via a smooth criterion, Automatic Control, IEEE Transactions on 54 (8) (2009) 1875–1880. doi:10.1109/TAC.2009.2020669.

[41] A. Isidori, Nonlinear Control Systems, Springer; 3rd edition, 1995.

[42] B. Morris, J. Grizzle, Hybrid invariant manifolds in systems with impulse effects with application to periodic locomotion in bipedal robots, Automatic Control, IEEE Transactions on 54 (8) (2009) 1751–1764. doi:10.1109/TAC.2009.2024563.

[43] E. Westervelt, J. Grizzle, D. Koditschek, Hybrid zero dynamics of planar biped walkers, Automatic Control, IEEE Transactions on 48 (1) (2003) 42–56. doi:10.1109/TAC.2002.806653.

[44] R. Gregg, J. Sensinger, Towards biomimetic virtual constraint control of a powered prosthetic leg, Control Systems Technology, IEEE Transactions on 22 (1) (2014) 246–254. doi:10.1109/TCST.2012.2236840.

[45] R. Gregg, T. Lenzi, L. Hargrove, J. Sensinger, Virtual constraint control of a powered prosthetic leg: From simulation to experiments with transfemoral amputees, Robotics, IEEE Transactions on 30 (6) (2014) 1455–1471. doi:10.1109/TRO.2014.2361937.

[46] C. Chevallereau, G. Abba, Y. Aoustin, F. Plestan, E. Westervelt, C. Canudas-de Wit, J. Grizzle, RABBIT: a testbed for advanced control theory, Control Systems Magazine, IEEE 23 (5) (2003) 57–79. doi:10.1109/MCS.2003.1234651.

[47] M. Maggiore, L. Consolini, Virtual holonomic constraints for Euler Lagrange systems, Automatic Control, IEEE Transactions on 58 (4) (2013) 1001–1008. doi:10.1109/TAC.2012.2215538.

[48] A. Shiriaev, A. Sandberg, C. Canudas de Wit, Motion planning and feedback stabilization of periodic orbits for an acrobot, in: Decision and Control. 43rd IEEE Conference on, Vol. 1, 2004, pp. 290–295 Vol.1. doi:10.1109/CDC.2004.1428645.

[49] J. Lack, M. Powell, A. Ames, Planar multi-contact bipedal walking using hybrid zero dynamics, in: Robotics and Automation, IEEE International Conference on, 2014, pp. 2582–2588. doi:10.1109/ICRA.2014.6907229.

[50] A. Martin, R. Gregg, Hybrid invariance and stability of a feedback linearizing controller for powered prostheses, in: American Control Conference, 2015, pp. 4670–4676.

[51] H. Zhao, J. Horn, J. Reher, V. Paredes, A. D. Ames, A hybrid systems and optimization-based control approach to realizing multi-contact locomotion on transfemoral prostheses, in: 54th IEEE Conference on Decision and Control, Osaka, Japan, 2015.

[52] Dynamic Leg Locomotion at University of Michigan, https://sites.google.com/site/atrias21/ (2013).

[53] C.-L. Shih, J. W. Grizzle, C. Chevallereau, From stable walking to steering of a 3D bipedal robot with passive point feet, Robotica 30 (2012) 1119–1130. doi:10.1017/S026357471100138X.

[54] D. Henrion, J. Lofberg, M. Kocvara, M. Stingl, Solving polynomial static output feedback problems with PENBMI, in: Decision and Control, and European Control Conference. 44th IEEE Conference on, 2005, pp. 7581–7586. doi:10.1109/CDC.2005.1583385.

[55] TOMLAB optimization, http://tomopt.com/tomlab/.

[56] J. Lofberg, YALMIP: a toolbox for modeling and optimization in MATLAB, in: Computer Aided Control Systems Design, 2004 IEEE International Symposium on, 2004, pp. 284–289.

[57] K. Akbari Hamed's YouTube Channel, Reduced-Order Framework for Stabilization of Periodic Orbits on Parameterized HZD Manifolds,

{https://www.youtube.com/watch?v=e_DlqFFCnf0&feature=youtu.be}

(2016).

[58] E. Westervelt, J. Grizzle, C. Chevallereau, J. Choi, B. Morris, Feedback Control of Dynamic Bipedal Robot Locomotion, Taylor & Francis/CRC, 2007.